



## Translated Paper

# Prediction of the peak seismic response of asymmetric buildings under bidirectional horizontal ground motion using equivalent SDOF model

Kenji Fujii 

Department of Architecture, Faculty of Creative Engineering, Chiba Institute of Technology, Narashino-shi Chiba, Japan

### Correspondence

Kenji Fujii, Department of Architecture, Faculty of Creative Engineering, Chiba Institute of Technology, Narashino-shi Chiba, Japan.  
Email: kenji.fujii@it-chiba.ac.jp

### Funding information

No funding information is provided.

The Japanese version of this paper was published in Volume 79, Number 706, pages 1783-1793, <https://doi.org/10.3130/aijs.79.1783> of *Journal of Structural and Construction Engineering (Transactions of AIJ)*. The authors have obtained permission for secondary publication of the English version in another journal from the Editor of *Journal of Structural and Construction Engineering (Transactions of AIJ)*. This paper is based on the translation of the Japanese version with some slight modifications.

Received June 30, 2017; Accepted September 16, 2017

doi: 10.1002/2475-8876.1007

### Abstract

The applicability of a simplified procedure, namely mode-adaptive bidirectional pushover analysis (MABPA), to the prediction of the non-linear peak response of a multistory asymmetric building subjected to bidirectional excitation is discussed. The first part of the paper summarizes the formulation of 2 independent equivalent single-degree-of-freedom models representing the first and second modal responses. The relationship between the critical assumptions of MABPA and the torsional index defined based on mode shape is then discussed. In the latter part of the paper, non-linear time-history analyses of 4-story torsionally stiff (TS) or torsionally flexible asymmetric buildings are described, and the results are compared with the predictions. The results show that MABPA predicts the peak response displacement of only the TS asymmetric buildings satisfactorily. Therefore, MABPA should be considered applicable only to TS buildings. The applicability of MABPA to a given asymmetric building may be evaluated by using the torsional indices of the first 3 modes.

### Keywords

bidirectional seismic input, equivalent SDOF model, mode-adaptive bidirectional pushover analysis, multistory asymmetric building model, torsional index

## 1. Introduction

### 1.1 Background

Buildings with highly irregular plans (hereinafter, asymmetric buildings) tend to be vulnerable to earthquakes.<sup>1-3</sup> When conducting a seismic assessment of an asymmetric building, the effect of simultaneous excitation should be considered properly: it is essential to perform 3-dimensional analyses that consider all possible directions of seismic inputs. The most rigorous method for evaluating the seismic response of a building is the non-linear dynamic (time-history) analysis of a multiple-degree-of-freedom (MDOF) model. However, this approach is very time consuming and requires huge computational effort to evaluate the response to all possible directions of seismic intensity and incidence of seismic input. Instead, simplified non-linear analytical procedures that combine the non-linear static (pushover) analysis of an MDOF model and the response spectrum analysis of an equivalent single-degree-of-freedom (SDOF) model are available.<sup>4-6</sup> Implemented widely in seismic design codes and seismic evaluation schemes,<sup>7-10</sup> these procedures work well for buildings that oscillate predominantly with a single mode.

In the author's opinion, non-linear time-history analyses may not be suitable for the common structural design work carried out in most design offices. Instead, the simplified procedures are more suitable for common structural designers and analysts. This is because such procedures provide basic information about the building being analyzed, thereby helping the designers and analysts to understand its non-linear seismic behavior such as its pushover curve and the non-linear properties of the equivalent SDOF model in the acceleration-displacement format.<sup>6</sup> Therefore, these simplified procedures must be extended to asymmetric buildings considering the effect of simultaneous excitation from all possible directions of the seismic input.

### 1.2 Review of previous work and problems to be investigated

The influence of the direction of incidence of the seismic input on the response of the building has been investigated previously, both analytically<sup>11-24</sup> and experimentally.<sup>25</sup> The results of these investigations suggest that the critical direction (ie, the one that produces the largest response) may not necessarily coincide with one of the main orthogonal axes of the building. To evaluate the largest response under bidirectional horizontal

excitation, López and Torres<sup>18</sup> proposed a method wherein the spectra of the major and minor components of horizontal ground motion are assumed identical.

In recent decades, the author and other researchers worked to extend these simplified procedures to improve the seismic-performance estimates of buildings with plan or elevation irregularities or both.<sup>26-55</sup> Recent investigations of the extension of this simplified procedure to an irregular structure were conducted by Lavan and De Stefano<sup>56</sup> and Zembaty and De Stefano.<sup>57</sup> The research over the past decade on the seismic behavior of irregular buildings were reviewed by De Stefano and Pintucchi<sup>58</sup> and Anagnostopoulos et al.<sup>59</sup> Most of those studies focused on extending the simplified procedure to asymmetric buildings with regular elevation, while a few studied asymmetric buildings with setbacks.<sup>27,30,36,55</sup>

From the author's point of view, there are 4 possible approaches to predict the peak response of an asymmetric building while considering torsional effects. The first is to combine non-linear pushover analysis and linear dynamic analysis.<sup>28-36</sup> The second is to combine non-linear pushover analysis (representing several modal responses) and either the square root of sum of squares (SRSS) or the complete quadratic combination (CQC), as proposed by Chopra and Goel.<sup>37-43</sup> The third approach is to combine 2 pushover analyses and envelope the results, as proposed by Bosco et al.<sup>44,45</sup> The fourth approach is to combine the analyses of 2 independent equivalent SDOF models (representing the first and second modes) and the envelope of 4 pushover analyses (including the effect of bidirectional excitation).<sup>50-55</sup>

The first approach, known as the *extended N2 method*, is the extended version of the simplified procedure proposed by Fajfar and Fischinger.<sup>5</sup> It involves estimating the peak response of each frame from pushover analysis results multiplied by a "correction factor" that is defined using linear dynamic analysis and pushover analysis results.<sup>28,29,31,32</sup> The extended N2 method has been examined and verified in various studies.<sup>30,33</sup> In this method, the elastic envelope of lateral displacement is assumed conservatively with respect to the inelastic envelope, as noted by De Stefano and Pintucchi.<sup>60</sup> They pointed out that this assumption may be invalid for structures characterized by very high torsional stiffness. Isakovic and Fischinger<sup>61</sup> performed shaking table tests on a reinforced concrete (RC) bridge structure and showed that the extended N2 method failed to estimate the peak response under high seismic intensity because it did not consider changes in the fundamental mode. Note that the latest version of the extended N2 method<sup>31,32</sup> assumes that (i) the correction factor in the vertical plane is independent of the position in the horizontal plane and (ii) the correction factor in the horizontal plane (torsional effect) is independent of the floor level and is determined based on the displacement at the roof (top floor). The latter assumption may be invalid for an asymmetric building with a setback, where the centers of mass of all the floors do not lie along the same vertical axis.

The second approach, known as *modal pushover analysis* (MPA), was proposed by Chopra and Goel<sup>62</sup> for regular buildings considering the effect of higher modes, and was then extended to asymmetric buildings.<sup>37</sup> It was extended further by Reyes and Chopra,<sup>38,39</sup> who considered the effect of bidirectional excitation. In MPA, the seismic response is estimated using (i) the pushover analysis of an MDOF model with an invariant force distribution based on each elastic mode shape, (ii) the estimation of the peak response of the independent equivalent SDOF models, and (iii) the combination rules that

are usually applied in linear analysis (ie, SRSS or CQC). However, Manoukas et al.<sup>40,41</sup> proposed a concept of the equivalent SDOF model that differed from that proposed by Chopra: Manoukas et al. considered the effect of bidirectional excitation in the formulation of the equivalent SDOF model. From the author's point of view, the applicability of MPA depends strongly on whether the mode shape changes significantly in the elastic range. To overcome the shortcoming of MPA, Belejo and Bento<sup>42</sup> applied an improved pushover analysis (IMPA)—a modified version of MPA that considers changes in mode shape in the inelastic regime—to buildings with 3 and 9 stories. It is interesting that the IMPA approximates the mode shape in the inelastic regime via several iterations of conventional (non-adaptive) force-based pushover, which may be easy to apply in common design work.

As proposed by Bosco et al.,<sup>44</sup> the third approach estimates the peak response of the frames on the stiff side and that of the frames on the flexible side by enveloping the results of 2 pushover analyses. Bosco et al. investigated the applicability of this procedure to multistory building models with the same geometry on each floor.<sup>45</sup> In this procedure, "corrective eccentricity" is the key parameter in the pushover analyses. This may be a promising approach because the various possible collapse mechanisms resulting from the combination of several modal responses can be properly predicted using a combination of different force distributions. However, because the corrective eccentricity is formulated using the parameters of a single-story building model, and because the reliability of its formulation relies strongly on the results of many numerical examples of single-story asymmetric building models, it may be difficult to apply this method to more general cases, such as a multistory building with dual systems (ie, a moment-resisting frame and structural walls) or various dampers, and multistory buildings with setbacks.

The fourth approach was proposed by the author.<sup>46-55</sup> In this article, this simplified procedure is called *mode-adaptive bidirectional pushover analysis* (MABPA). It involves evaluating the peak responses of the first and second modes independently from the equivalent SDOF models formulated considering the principal direction of the first modal response. The prediction of the peak response at each frame is based on a set of pushover analyses considering the combination of the 2 modal responses. The first version of MABPA<sup>50</sup> was applicable only to asymmetric buildings with regular elevation and the same geometry on each floor designed according to the weak-beam/strong-column concept. This was because a conversion step was required from the multistory building model to an equivalent single-story model. However, in the latest version of MABPA,<sup>53</sup> the following 3 modifications were made. First, the multistory building model can now be converted directly to equivalent SDOF models because of the development of displacement-based mode-adaptive pushover (DB-MAP) analysis for a multistory frame structure, which can account for changes in the mode shape at each non-linear stage. Second, for the conservative prediction of the largest peak response considering all possible incident directions of seismic input, the spectra of the major and minor components of horizontal ground motion are assumed identical. Third, for obtaining better estimates when the change in the principal direction of the first modal response beyond the elastic regime is significant, this change is considered in each non-linear stage. Note that the second modification, namely, the identical-component assumption, is the same as that discussed by López and Torres<sup>18</sup> for elastic spectrum analysis. This latest version of

MABPA successfully predicted the peak response of asymmetric buildings with hysteresis dampers,<sup>54</sup> in which the change in the mode shape beyond the elastic regime was significant. It also predicted the peak response of asymmetric buildings with bidirectional setbacks designed according to the weak beam/strong column concept.<sup>55</sup>

Although the latest version of MABPA can successfully predict the peak response of asymmetric buildings, it requires 2 critical assumptions. The first is that the building oscillates predominantly in a single mode in each set of orthogonal directions, and the second is that the principal directions of the first and second modal responses are almost orthogonal. Previous work on a single-story asymmetric building model<sup>63</sup> has shown that these assumptions may be valid when the building in question is torsionally stiff (TS) in both orthogonal directions, but these 2 assumptions are invalid for most torsionally flexible (TF) structures. However, when assessing the applicability of MABPA to a given asymmetric multistory building, another problem arises. According to Hajal and Chopra,<sup>64</sup> a structure is classified as TS or TF based on  $\Omega_0$ , the ratio of the uncoupled torsional circular frequency with respect to the center of stiffness to the uncoupled lateral circular frequency of the torsionally balanced system. Unfortunately,  $\Omega_0$  can be evaluated rigorously only for single-story asymmetric buildings (and multistory asymmetric buildings that satisfy certain conditions). Another finding from a previous work<sup>63</sup> is that the torsional index  $R_{\rho i}$  of each mode is a key parameter in classifying a structure as TS or TF. For all TS systems analyzed in the previous work,<sup>63</sup> the torsional indices  $R_{\rho 1}$  and  $R_{\rho 2}$  of the first and second modes, respectively, were less than unity, whereas the torsional index of the third mode ( $R_{\rho 3}$ ) was greater than unity. Therefore, the expectation is that the torsional indices can provide a quantitative way to assess the applicability of MABPA to a given multistory asymmetric building model. This problem is investigated in the present work.

### 1.3 Objectives

In this article, the ability of MABPA<sup>53</sup> to predict the peak response of TS and TF asymmetric buildings with regular elevation is assessed, and the limitations of MABPA are discussed based on the torsional indices of the first 3 modes.

In Section 2, 2 independent equivalent SDOF models representing the first and second modal responses are formulated. This is followed by a discussion on the relationship between the critical assumptions of MABPA and the torsional index based on mode shapes. In Section 3, non-linear time-history analyses of 3 four-story TS and TF asymmetric buildings are described, and the results are compared with predictions. In Section 4, a quantitative assessment of the applicability of MABPA to 6 asymmetric building models using the torsional indices of the first 3 modes is presented.

Note that this article focuses on the accuracy of MABPA for predicting the peak responses of TS and TF asymmetric buildings, and that only the case in which the spectra of the major and minor components of horizontal ground motion are identical is considered. Hence, there is no discussion regarding the influence of the incident direction of seismic input on the responses of TS and TF asymmetric buildings.

## 2. Description of MABPA

### 2.1 Equations of the equivalent SDOF model

The equations of motion of the equivalent SDOF model representing the first and second modal responses are formulated

below.<sup>53</sup> Figure 1 shows a plan view of the multistory asymmetric building model with  $N$  stories.

Considering a set of  $\xi$  and  $\zeta$  axes in the  $X$ - $Y$  plane and the angle  $\psi$  as shown in Figure 1, the equations of motion for an  $N$ -story asymmetric-frame building model can be written as follows:

$$\mathbf{M}\ddot{\mathbf{d}}(t) + \mathbf{C}\dot{\mathbf{d}}(t) + \mathbf{f}_R(t) = -\mathbf{M}\{\alpha_\xi a_{g\xi}(t) + \alpha_\zeta a_{g\zeta}(t)\}, \quad (1)$$

$$\mathbf{M} = \begin{bmatrix} \mathbf{M}_0 & \mathbf{0} & \mathbf{0} \\ \mathbf{0} & \mathbf{M}_0 & \mathbf{0} \\ \mathbf{0} & \mathbf{0} & \mathbf{I}_0 \end{bmatrix}, \mathbf{M}_0 = \begin{bmatrix} m_1 & & 0 \\ & \ddots & \\ 0 & & m_N \end{bmatrix}, \mathbf{I}_0 = \begin{bmatrix} I_1 & & 0 \\ & \ddots & \\ 0 & & I_N \end{bmatrix}, \quad (2)$$

$$\begin{cases} \mathbf{d} = \{x_1 \cdots x_N \ y_1 \cdots y_N \ \theta_1 \cdots \theta_N\}^T \\ \mathbf{f}_R = \{f_{RX1} \cdots f_{RXN} \ f_{RY1} \cdots f_{RYN} \ f_{MZ1} \cdots f_{MZN}\}^T, \end{cases} \quad (3)$$

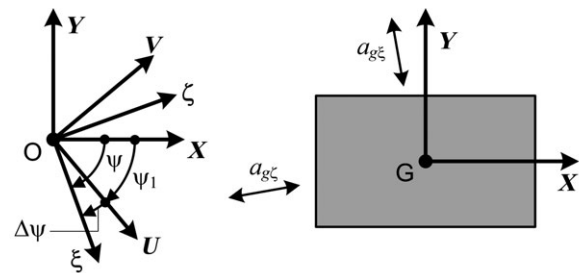
$$\begin{cases} \alpha_\xi = \{\cos \psi \cdots \cos \psi \ -\sin \psi \cdots -\sin \psi \ 0 \cdots 0\}^T \\ \alpha_\zeta = \{\sin \psi \cdots \sin \psi \ \cos \psi \cdots \cos \psi \ 0 \cdots 0\}^T \end{cases} \quad (4)$$

In Equation (1),  $\mathbf{M}$  is the mass matrix;  $\mathbf{C}$  is the damping matrix;  $\mathbf{d}(t)$  and  $\mathbf{f}_R(t)$  are the displacement and restoring force vectors, respectively;  $a_{g\xi}$  and  $a_{g\zeta}$  are the ground accelerations of the  $\xi$  and  $\zeta$  components, respectively; and  $m_j$  and  $I_j$  are the mass and mass moment of inertia of the  $j$ -th floor, respectively.

Let  $\phi_i$  in Equation (5) be the  $i$ -th mode vector of an asymmetric building:

$$\phi_i = \{\phi_{X1i} \cdots \phi_{XNi} \ \phi_{Y1i} \cdots \phi_{YNi} \ \phi_{\Theta 1i} \cdots \phi_{\Theta Ni}\}^T. \quad (5)$$

In Equation (5),  $\phi_{Xji}$ ,  $\phi_{Yji}$ , and  $\phi_{\Theta ji}$  are the  $X$ -,  $Y$ -, and rotational components, respectively, of the  $i$ -th mode vector at the  $j$ -th floor. In this article, a “purely translational mode” is defined as one whose rotational components  $\phi_{\Theta ji}$  are 0 at



**G** : Center of Mass  
**X, Y** : Set of Orthogonal Axes Corresponds to the Building's Main Orthogonal Axes  
**U, V** : Set of Orthogonal Axes Corresponds to the Building's Principal Direction of the First Modal Response. (U-axis is the principal direction of the first modal response.)  
**xi, zeta** : Set of Orthogonal Axes Corresponds to the Major/Minor Components of Seismic Input (xi-axis is the direction of major components, while zeta-axis is the direction of minor components.)

Figure 1. Plan view of an asymmetric building

every floor, and a “purely torsional mode” is defined as one whose translational components  $\phi_{xji}$  and  $\phi_{yji}$  are 0 at every floor. The tangent of  $\psi_i$ , the angle of incidence of the principal axis of the  $i$ -th modal response with respect to  $X$ -axis, is

$$\tan \psi_i = -\frac{\sum_j m_j \phi_{yji}}{\sum_j m_j \phi_{xji}}. \quad (6)$$

From Equation (6), the cosine and sine of  $\psi_i$  are written as

$$\begin{cases} \cos \psi_i = \frac{\sum_j m_j \phi_{xji}}{\sqrt{\left(\sum_j m_j \phi_{xji}\right)^2 + \left(\sum_j m_j \phi_{yji}\right)^2}} \\ \sin \psi_i = -\frac{\sum_j m_j \phi_{yji}}{\sqrt{\left(\sum_j m_j \phi_{xji}\right)^2 + \left(\sum_j m_j \phi_{yji}\right)^2}} \end{cases}. \quad (7)$$

Let the  $U$ -axis be the principal axis of the first modal response, with the  $V$ -axis orthogonal to it, as shown in Figure 1. To formulate the equations of motion of the 2 equivalent SDOF models, the following 4 assumptions are made.

**Assumption 1.** The principal directions of the first and second modal responses are almost orthogonal. In other words, the principal direction of the second modal response is almost identical to the  $V$ -axis.

**Assumption 2.** The building oscillates predominantly in the first mode under  $U$ -directional (unidirectional) excitation, and predominantly in the second mode under  $V$ -directional excitation.

**Assumption 3.** Assumption 2 remains valid even if the building oscillates beyond the elastic range if the change in the mode vector in the non-linear stage is properly considered and the  $U$ -axis is properly modified to correspond to the first mode vector in the non-linear stage.

**Assumption 4.** Under bidirectional excitation, the response of the building can be approximated by the sum of the contributions of the first and second modal responses even if the building oscillates beyond the elastic range.

From assumption 4, the displacement vector  $\mathbf{d}(t)$  and restoring force  $\mathbf{f}_R(t)$  can be written as

$$\begin{cases} \mathbf{d}(t) = \Gamma_{1U} \boldsymbol{\phi}_1 D_{1U}^*(t) + \Gamma_{2V} \boldsymbol{\phi}_2 D_{2V}^*(t) \\ \mathbf{f}_R(t) = \mathbf{M} \{ \Gamma_{1U} \boldsymbol{\phi}_1 A_{1U}^*(t) + \Gamma_{2V} \boldsymbol{\phi}_2 A_{2V}^*(t) \}. \end{cases} \quad (8)$$

In Equation (8),  $\Gamma_{1U}$  is the participation factor of the first mode with respect to the  $U$ -axis, and  $\Gamma_{2V}$  is that of the second mode with respect to the  $V$ -axis:

$$\Gamma_{1U} = \frac{\boldsymbol{\phi}_1^T \mathbf{M} \boldsymbol{\alpha}_U}{\boldsymbol{\phi}_1^T \mathbf{M} \boldsymbol{\phi}_1}, \quad \Gamma_{2V} = \frac{\boldsymbol{\phi}_2^T \mathbf{M} \boldsymbol{\alpha}_V}{\boldsymbol{\phi}_2^T \mathbf{M} \boldsymbol{\phi}_2}, \quad (9)$$

$$\begin{cases} \boldsymbol{\alpha}_U = \{ \cos \psi_1 \ \cdots \ \cos \psi_1 \ -\sin \psi_1 \ \cdots \ -\sin \psi_1 \ 0 \ \cdots \ 0 \}^T \\ \boldsymbol{\alpha}_V = \{ \sin \psi_1 \ \cdots \ \sin \psi_1 \ \cos \psi_1 \ \cdots \ \cos \psi_1 \ 0 \ \cdots \ 0 \}^T \end{cases} \quad (10)$$

The equivalent displacement  $D_{1U}^*(t)$  and acceleration  $A_{1U}^*(t)$  of the first modal response with respect to the  $U$ -axis are defined in Equation (11), while those of the second modal response with respect to the  $V$ -axis are defined in Equation (12):

$$D_{1U}^*(t) = \frac{\Gamma_{1U} \boldsymbol{\phi}_1^T \mathbf{M} \mathbf{d}(t)}{M_{1U}^*}, \quad A_{1U}^*(t) = \frac{\Gamma_{1U} \boldsymbol{\phi}_1^T \mathbf{f}_R(t)}{M_{1U}^*}, \quad (11)$$

$$D_{2V}^*(t) = \frac{\Gamma_{2V} \boldsymbol{\phi}_2^T \mathbf{M} \mathbf{d}(t)}{M_{2V}^*}, \quad A_{2V}^*(t) = \frac{\Gamma_{2V} \boldsymbol{\phi}_2^T \mathbf{f}_R(t)}{M_{2V}^*}, \quad (12)$$

$$M_{1U}^* = \Gamma_{1U}^2 \boldsymbol{\phi}_1^T \mathbf{M} \boldsymbol{\phi}_1, \quad M_{2V}^* = \Gamma_{2V}^2 \boldsymbol{\phi}_2^T \mathbf{M} \boldsymbol{\phi}_2. \quad (13)$$

In Equation (13),  $M_{1U}^*$  is the effective (equivalent) modal mass of the first mode with respect to the  $U$ -axis, and  $M_{2V}^*$  is the effective modal mass of the second mode with respect to the  $V$ -axis. Note that the cosine and sine of  $\psi_i$  in Equation (10) depend on the first mode vector  $\boldsymbol{\phi}_1$ , as shown in Equation (7): from assumption 3, the direction of the  $U$ -axis varies as the first mode vector  $\boldsymbol{\phi}_1$  changes in the non-linear range.

The equivalent damping coefficient  $C_{1U}^*$  of the first mode with respect to the  $U$ -axis, and that of the second mode with respect to  $V$ -axis, namely  $C_{2V}^*$ , are defined as

$$C_{1U}^* = \Gamma_{1U}^2 \boldsymbol{\phi}_1^T \mathbf{C} \boldsymbol{\phi}_1, \quad C_{2V}^* = \Gamma_{2V}^2 \boldsymbol{\phi}_2^T \mathbf{C} \boldsymbol{\phi}_2. \quad (14)$$

By substituting Equation (8) into Equation (1), Equation (15) is obtained:

$$\begin{aligned} & \mathbf{M} \{ \Gamma_{1U} \boldsymbol{\phi}_1 \ddot{D}_{1U}^*(t) + \Gamma_{2V} \boldsymbol{\phi}_2 \ddot{D}_{2V}^*(t) \} \\ & + \mathbf{C} \{ \Gamma_{1U} \boldsymbol{\phi}_1 \dot{D}_{1U}^*(t) + \Gamma_{2V} \boldsymbol{\phi}_2 \dot{D}_{2V}^*(t) \} \\ & + \mathbf{M} \{ \Gamma_{1U} \boldsymbol{\phi}_1 A_{1U}^*(t) + \Gamma_{2V} \boldsymbol{\phi}_2 A_{2V}^*(t) \} \\ & = -\mathbf{M} \{ \boldsymbol{\alpha}_\xi a_{g\xi}(t) + \boldsymbol{\alpha}_\zeta a_{g\zeta}(t) \} \end{aligned} \quad (15)$$

By multiplying both sides of Equation (15) by vector  $\Gamma_{1U} \boldsymbol{\phi}_1^T$  from the left-hand side, and considering Eqs. (16) and (17), the equation of motion of the equivalent SDOF model representing the first modal response is obtained as shown in Equation (18):

$$\boldsymbol{\phi}_1^T \mathbf{M} \boldsymbol{\phi}_2 = 0, \quad \boldsymbol{\phi}_1^T \mathbf{C} \boldsymbol{\phi}_2 \approx 0, \quad (16)$$

$$\begin{cases} \cos \Delta\psi = \cos(\psi - \psi_1) = \frac{\boldsymbol{\phi}_1^T \mathbf{M} \boldsymbol{\alpha}_\xi}{\boldsymbol{\phi}_1^T \mathbf{M} \boldsymbol{\alpha}_U} \\ \sin \Delta\psi = \sin(\psi - \psi_1) = \frac{\boldsymbol{\phi}_1^T \mathbf{M} \boldsymbol{\alpha}_\zeta}{\boldsymbol{\phi}_1^T \mathbf{M} \boldsymbol{\alpha}_U} \end{cases}, \quad (17)$$

$$\begin{aligned} & \ddot{D}_{1U}^*(t) + \frac{C_{1U}^*}{M_{1U}^*} \dot{D}_{1U}^*(t) + A_{1U}^*(t) \\ & = -\{ a_{g\xi}(t) \cos \Delta\psi + a_{g\zeta}(t) \sin \Delta\psi \}. \end{aligned} \quad (18)$$

Figure 2 shows the equivalent SDOF model for the first modal response.

The ground acceleration component  $a_{gU}(t)$  along the  $U$ -axis is defined as

$$a_{gU}(t) = a_{g\xi}(t) \cos \Delta\psi + a_{g\zeta}(t) \sin \Delta\psi. \quad (19)$$

Therefore, Equation (18) can be simplified as

$$\ddot{D}_{1U}^*(t) + \frac{C_{1U}^*}{M_{1U}^*} \dot{D}_{1U}^*(t) + A_{1U}^*(t) = -a_{gU}(t). \quad (20)$$

The equation of motion of the equivalent SDOF model representing the second modal response is derived in the same manner. By multiplying both sides of Equation (15) by vector  $\Gamma_{2V} \boldsymbol{\phi}_2^T$  from the left-hand side and considering Equation (16),

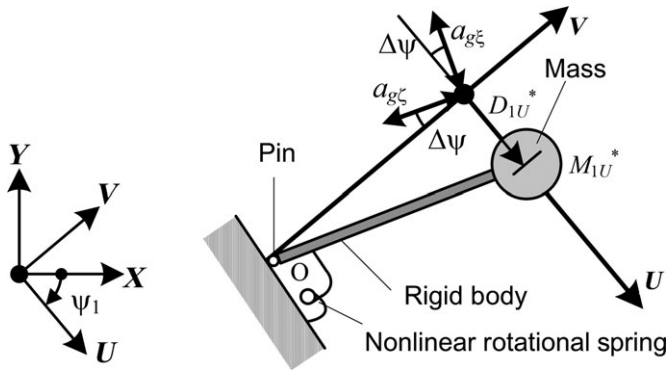


Figure 2. Equivalent SDOF model (the first mode)

the following equation can be obtained:

$$\ddot{D}_{2V}^*(t) + \frac{C_{2V}^*}{M_{2V}^*} \dot{D}_{2V}^*(t) + A_{2V}^*(t) = - \left\{ \frac{\varphi_2^T M \alpha_\xi}{\varphi_2^T M \alpha_V} a_{g\xi}(t) + \frac{\varphi_2^T M \alpha_\zeta}{\varphi_2^T M \alpha_V} a_{g\zeta}(t) \right\} \quad (21)$$

Let  $\psi_2$  be the angle of incidence of the principal direction of the second modal response with respect to the  $X$ -axis. Assumption 1 can then be expressed as:

$$(\tan \psi_1)(\tan \psi_2) \approx 1. \quad (22)$$

From Equations (6) and (22), Equation (23) is obtained:

$$\sum_j m_j \phi_{Yj2} / \sum_j m_j \phi_{Xj2} = -\tan \psi_2 \approx \frac{1}{\tan \psi_1} = \frac{\cos \psi_1}{\sin \psi_1}. \quad (23)$$

Therefore, the following relationship is obtained:

$$\begin{cases} \frac{\varphi_2^T M \alpha_\xi}{\varphi_2^T M \alpha_V} \approx -\sin \Delta\psi \\ \frac{\varphi_2^T M \alpha_\zeta}{\varphi_2^T M \alpha_V} \approx \cos \Delta\psi \end{cases} \quad (24)$$

By substituting Equation (24) into Equation (21) and considering Equation (25), the equation of motion of the equivalent SDOF model representing the second modal response is obtained as:

$$a_{gV}(t) = -a_{g\xi}(t) \sin \Delta\psi + a_{g\zeta}(t) \cos \Delta\psi, \quad (25)$$

$$\ddot{D}_{2V}^*(t) + \frac{C_{2V}^*}{M_{2V}^*} \dot{D}_{2V}^*(t) + A_{2V}^*(t) = -a_{gV}(t). \quad (26)$$

In Equation (25),  $a_{gV}(t)$  is the ground acceleration component along the  $V$ -axis.

## 2.2 Torsional index based on each modal shape

The following discussion focuses on the relationship between assumptions 1 and 2 described in section 2.1 and the torsional index based on each modal shape, as presented previously.<sup>25,53,63</sup> The torsional index  $R_{\rho i}$  of the  $i$ -th mode is defined as:

$$R_{\rho i} = \sqrt{\sum_j I_j \phi_{\Theta j i}^2 / \left( \sum_j m_j \phi_{Xj i}^2 + \sum_j m_j \phi_{Yj i}^2 \right)}. \quad (27)$$

From Equation (27), it is obvious that  $R_{\rho i}$  equals to 0 when the  $i$ -th mode is the purely translational mode, whereas  $R_{\rho i}$

becomes infinite when the  $i$ -th mode is the purely torsional mode. Therefore, the terms “predominantly translational” and “predominantly torsional” can be defined using  $R_{\rho i}$ : a “predominantly translational” mode is one for which  $R_{\rho i} < 1$ , whereas a “predominantly torsional” mode is one for which  $R_{\rho i} > 1$ .

A previous study of a single-story asymmetric building model<sup>63</sup> investigated the relationship between the model parameters and the torsional indices of the 3 modes. The parameters of a single-story asymmetric building model are (i) the eccentricity ratios  $E_X$  and  $E_Y (=e_X/r$  and  $e_Y/r$ , respectively, where  $e_X$  and  $e_Y$  are the stiffness eccentricities, and  $r$  is the radius of gyration of mass with respect to the center of mass) and (ii) the radius ratios  $J_X$  and  $J_Y$  of gyration of torsional stiffness with respect to the center of stiffness in each orthogonal direction ( $=j_X/r$  and  $j_Y/r$ , respectively, where  $j_X$  and  $j_Y$  are the radii of gyration of torsional stiffness with respect to the center of mass). The results of numerical investigations have shown that the torsional indices  $R_{\rho i}$  ( $i = 1-3$ ) of the 3 modes depend strongly on the radius ratios  $J_X$  and  $J_Y$ . In the case of an asymmetric building model for which both  $J_X$  and  $J_Y$  are greater than unity, both  $R_{\rho 1}$  and  $R_{\rho 2}$  are less than unity, and  $R_{\rho 3}$  is greater than unity. In contrast, in the case of an asymmetric building model for which both  $J_X$  and  $J_Y$  are less than unity,  $R_{\rho 1}$  is greater than unity, and both  $R_{\rho 2}$  and  $R_{\rho 3}$  are less than unity. In other words, when  $J_X$  and  $J_Y$  are both greater than unity, the first and second modes are predominantly translational, whereas the third mode is predominantly torsional.

Note that, in general, a system is classified as either TS or TF according to the definition by Hajal and Chopra,<sup>64</sup> which is based on  $\Omega_0$ . However, in the present study, the classification is made using the torsional indices  $R_{\rho 1}$  and  $R_{\rho 2}$  of the first and second modes as in a previous study<sup>53</sup> because  $\Omega_0$  can be evaluated rigorously only for single-story asymmetric buildings (and multistory asymmetric buildings that satisfy certain conditions). Herein, a building is classified as TS if  $R_{\rho 1}, R_{\rho 2} < 1$  and  $R_{\rho 3} > 1$ , or as TF if  $R_{\rho 1} > 1$  and  $R_{\rho 2}, R_{\rho 3} < 1$ .

First, the relationship between (i) the effective first modal mass ratio  $m_{1U}^*$  with respect to the  $U$ -axis and (ii) the torsional index  $R_{\rho 1}$  of the first mode is investigated. From Eqs. (7), (9), (13), and (27),  $m_{1U}^*$  can be expressed as:

$$m_{1U}^* = \frac{M_{1U}^*}{\sum_j m_j} = \frac{1}{\sum_j m_j} \cdot \frac{\left( \sum_j m_j \phi_{Xj1} \right)^2 + \left( \sum_j m_j \phi_{Yj1} \right)^2}{\sum_j m_j \phi_{Xj1}^2 + \sum_j m_j \phi_{Yj1}^2} \cdot \frac{1}{1 + R_{\rho 1}^2}. \quad (28)$$

This equation reveals that  $m_{1U}^*$  decreases if the first mode is predominantly torsional ( $R_{\rho 1} > 1$ ). Therefore, if the building oscillates predominantly in the first mode under  $U$ -directional (unidirectional) excitation, the first mode must be predominantly translational ( $R_{\rho 1} < 1$ ).

Next, the relationship between (i) the effective second modal mass ratio  $m_{2V}^*$  with respect to the  $V$ -axis and (ii) the torsional index  $R_{\rho 2}$  of the second mode is investigated. The angle of incidence  $\psi_2$  of the principal direction of the second mode is related to  $\psi_1$  as follows:

$$\psi_2 = \psi_1 + \Delta\psi_{12}. \quad (29)$$

In Equation (29),  $\Delta\psi_{12}$  is the angle between the principal directions of the first and second modes. From Eqs. (7), (9),

(10), (13), (27), and (29),  $m_{2V}^*$  can be expressed as:

$$m_{2V}^* = \frac{M_{2V}^*}{\sum_j m_j} = \frac{1}{\sum_j m_j} \cdot \frac{\left(\sum_j m_j \phi_{Xj2}\right)^2 + \left(\sum_j m_j \phi_{Yj2}\right)^2}{\sum_j m_j \phi_{Xj2}^2 + \sum_j m_j \phi_{Yj2}^2} \cdot \frac{1}{1 + R_{\rho2}^2} \cdot \sin^2(\Delta\psi_{12}). \quad (30)$$

This equation reveals that  $m_{2V}^*$  decreases if the second mode is predominantly torsional ( $R_{\rho2} > 1$ ) or the sine of  $\Delta\psi_{12}$  is far from unity. Therefore, if the building oscillates predominantly in the second mode under V-directional excitation, the second mode must be predominantly translational ( $R_{\rho2} < 1$ ) and the sine of  $\Delta\psi_{12}$  must be close to unity. In summary, if assumption 2 is suitable for an asymmetric building, the torsional indices  $R_{\rho1}$  and  $R_{\rho2}$  of its first and second modes must be less than unity and the sine of  $\Delta\psi_{12}$  must be close to unity.

Next, the relationship between the angle  $\Delta\psi_{12}$  and the torsional indices  $R_{\rho1}$  and  $R_{\rho2}$  is discussed. As shown in a previous work,<sup>63</sup> the following interesting relationship exists for a single-story asymmetric building model:

$$|\cos \Delta\psi_{12}| = R_{\rho1} R_{\rho2}. \quad (31)$$

This equation is valid only for single-story buildings and multistory asymmetric buildings that satisfy certain conditions. However, Equation (31) suggests that the product  $R_{\rho1} R_{\rho2}$  must be close to 0 if assumption 1 is applicable to the asymmetric building in question. As discussed above, the effective modal mass ratios  $m_{1U}^*$  and  $m_{2V}^*$  increase as  $R_{\rho1}$  and  $R_{\rho2}$  approach 0. Therefore, if assumptions 1 and 2 both are applicable,  $R_{\rho1}$  and  $R_{\rho2}$  must be less than unity, and the product  $R_{\rho1} R_{\rho2}$  must be close to 0. In other words, if assumptions 1 and 2 both are applicable to a given asymmetric building, it must be a TS building that satisfies the conditions  $R_{\rho1}, R_{\rho2} < 1$  and  $R_{\rho3} > 1$ .

## 2.3 Outline of MABPA<sup>53</sup>

### 2.3.1 Step 1: Pushover analysis of the asymmetric building model (the first mode)

The non-linear properties of the equivalent SDOF model representing the first modal response, namely, the relationship between the equivalent acceleration  $A_{1U}^*$  and equivalent displacement  $D_{1U}^*$ , referred to as the capacity curve, are determined by the pushover analysis. In this analysis, the change in shape of the first mode at each non-linear stage is considered. In this article, DB-MAP analysis<sup>53</sup> is applied.

The equivalent displacement  ${}_n D_{1U}^*$  and acceleration  ${}_n A_{1U}^*$  at each loading step  $n$  are determined from Eqs. (32) and (33), assuming that the displacement vector  ${}_n \mathbf{d}$  at each loading stage is proportional to the first mode vector  ${}_n \Gamma_{1U} {}_n \Phi_1$  at each loading stage:

$${}_n D_{1U}^* = \frac{{}_n \Gamma_{1U} {}_n \Phi_1^T {}_n \mathbf{M} \mathbf{d}}{{}_n M_{1U}^*} = \frac{\sum_j (m_{jn} x_j^2 + m_{jn} y_j^2 + I_{jn} \theta_j^2)}{\sqrt{\left(\sum_j m_{jn} x_j\right)^2 + \left(\sum_j m_{jn} y_j\right)^2}}, \quad (32)$$

$${}_n A_{1U}^* = \frac{{}_n \Gamma_{1U} {}_n \Phi_1^T {}_n \mathbf{f}_R}{{}_n M_{1U}^*} = \frac{\sum_j ({}_n f_{RXjn} x_j + {}_n f_{RYjn} y_j + {}_n f_{MZjn} \theta_j)}{\sqrt{\left(\sum_j m_{jn} x_j\right)^2 + \left(\sum_j m_{jn} y_j\right)^2}}, \quad (33)$$

$$\begin{cases} {}_n \mathbf{d} = \{ {}_n x_1 \cdots {}_n x_N \quad {}_n y_1 \cdots {}_n y_N \quad {}_n \theta_1 \cdots {}_n \theta_N \}^T \\ {}_n \mathbf{f}_R = \{ {}_n f_{RX1} \cdots {}_n f_{RXN} \quad {}_n f_{RY1} \cdots {}_n f_{RYN} \quad {}_n f_{MZ1} \cdots {}_n f_{MZN} \}^T \end{cases} \quad (34)$$

### 2.3.2 Step 2: Prediction of the peak seismic response of the equivalent SDOF model (the first mode)

The largest peak equivalent displacement  $D_{1U}^*{}_{\max}$  and equivalent acceleration  $A_{1U}^*{}_{\max}$  are obtained from the given response spectrum of ground motion (the relationship between pseudo-spectral acceleration  ${}_p S_A$  and spectral displacement  $S_d$ ) and the capacity curve obtained in Step 1 using the equivalent linearization technique.<sup>64</sup> The equivalent period  ${}_n T_{1eq}$  and equivalent damping ratio  ${}_n h_{1eq}$  of the equivalent SDOF model at each loading step  $n$  are determined as:

$${}_n T_{1eq} = 2\pi \sqrt{{}_n D_{1U}^* / {}_n A_{1U}^*} \cdot {}_n h_{1eq} = \sum_k ({}_n h_{eqk} \cdot {}_n W_{ek}) / \sum_k {}_n W_{ek}, \quad (35)$$

$${}_n h_{eqk} = \begin{cases} h_0 \sqrt{{}_n K_{EQk} / K_{Ek}} & : {}_n \mu_k < 1 \\ 0.25(1 - 1/\sqrt{{}_n \mu_k}) + h_0 \sqrt{{}_n K_{EQk} / K_{Ek}} & : {}_n \mu_k \geq 1 \end{cases} \quad (36)$$

In Eqs. (35) and (36),  ${}_n h_{eqk}$ ,  ${}_n W_{ek}$ , and  ${}_n \mu_k$  are the equivalent damping ratio, potential energy, and ductility ratio, respectively, of the  $k$ -th non-linear spring;  ${}_n K_{EQk}$  and  $K_{Ek}$  are the equivalent (secant) stiffness at step  $n$  and initial stiffness, respectively, of the  $k$ -th non-linear spring; and  $h_0$  is the initial damping ratio, which is assumed as 0.03 in this work. Note that an antisymmetric curvature distribution is assumed for beams and columns to calculate  ${}_n W_{ek}$ , whereas a symmetric curvature distribution is assumed for structural walls. Note that Equation (36) is modified from the equation shown in reference,<sup>65,66</sup> considering the damping proportional to instant stiffness as discussed by Yoshikawa et al.<sup>67</sup>

The spectral reduction factor  $F({}_n h_{1eq})$  relating to the equivalent damping ratio  ${}_n h_{1eq}$  is determined as:

$$F({}_n h_{1eq}) = \frac{{}_p S_A({}_n T_{1eq}, {}_n h_{1eq})}{{}_p S_A({}_n T_{1eq}, 0.05)} = \frac{S_D({}_n T_{1eq}, {}_n h_{1eq})}{S_D({}_n T_{1eq}, 0.05)} = \frac{1.5}{1 + 10h_{1eq}}. \quad (37)$$

In Equation (37),  ${}_p S_A({}_n T_{1eq}, {}_n h_{1eq})$  and  $S_D({}_n T_{1eq}, {}_n h_{1eq})$  are the pseudo-spectral acceleration and spectral displacement, respectively, of the ground motion. In this study, the relationship between  ${}_p S_A({}_n T_{1eq}, {}_n h_{1eq})$  and  $S_D({}_n T_{1eq}, {}_n h_{1eq})$  is referred to as the demand curve. To predict the "largest" peak response, the same response spectra are used to predict the peak responses of the first and second modes. The predicted peak responses ( $D_{1U}^*{}_{\max}$  and  $A_{1U}^*{}_{\max}$ ) are obtained as the intersection point of the capacity and demand curves. Alternatively, the other equivalent linearization technique and the inelastic response spectrum

given in some codes<sup>6,10</sup> may be used to obtain the peak response of the equivalent SDOF model.

### 2.3.3 Step 3: Pushover analysis of the asymmetric building model (the second mode)

From the results of steps 1 and 2, the first mode vector corresponding to  $D_{1U}^*$ , namely,  $\Gamma_{1Uie}\Phi_{1ie}$ , is obtained. The second mode vector, namely,  $\Gamma_{2Vie}\Phi_{2ie}$ , is then determined from Equation (38) in terms of  $\Gamma_{1Uie}\Phi_{1ie}$  and the second mode vector in the elastic range, namely,  $\Phi_{2e}$ , considering the orthogonality of the mode vectors:

$$\Gamma_{2Vie} = \frac{\Phi_{2ie}^T \mathbf{M} \alpha_{vie}}{\Phi_{2ie}^T \mathbf{M} \Phi_{2ie}}, \Phi_{2ie} = \Phi_{2e} - \frac{\Phi_{2e}^T \mathbf{M} \Phi_{1ie}}{\Phi_{1ie}^T \mathbf{M} \Phi_{1ie}} \Phi_{1ie}, \quad (38)$$

$$\alpha_{vie} = \{\sin \psi_{1ie} \cdots \sin \psi_{1ie} \cos \psi_{1ie} \cdots \cos \psi_{1ie} \ 0 \cdots 0\}^T. \quad (39)$$

Next, another pushover analysis of an MDOF model is carried out to obtain the force-displacement relationship representing the second mode response by applying the invariant force distribution  $\mathbf{p}_2$  determined as:

$$\mathbf{p}_2 = \mathbf{M}(\Gamma_{2Vie}\Phi_{2ie}). \quad (40)$$

The equivalent displacement  ${}_n D_{2V}^*$  and acceleration  ${}_n A_{2V}^*$  of the equivalent SDOF model representing the second modal response at each loading step  $n$  are determined by

$${}_n D_{2V}^* = \frac{\Gamma_{2Vie}\Phi_{2ie}^T \mathbf{M} \mathbf{n} \mathbf{d}}{M_{2Vie}^*}, {}_n A_{2V}^* = \frac{\Gamma_{2Vie}\Phi_{2ie}^T \mathbf{M} \mathbf{n} \mathbf{f}_R}{M_{2Vie}^*}, \quad (41)$$

$$M_{2Vie}^* = \Gamma_{2Vie}^2 \Phi_{2ie}^T \mathbf{M} \Phi_{2ie}. \quad (42)$$

In Equation (42),  $M_{2Vie}^*$  is the equivalent second modal mass with respect to the  $V$ -axis, and it is determined in terms of  $\Gamma_{2Vie}\Phi_{2ie}$ .

### 2.3.4 Step 4: Prediction of peak seismic response of the equivalent SDOF model (the second mode)

The largest peak equivalent displacement  $D_{2V}^*_{\max}$  and the equivalent acceleration  $A_{2V}^*_{\max}$  for the second modal response are obtained using the equivalent linearization technique as discussed in step 2. Note that the spectrum used in step 2 is again used to predict the second mode response.

### 2.3.5 Step 5: Prediction of the largest peak seismic response at each frame

From the results of steps 2 and 4, 4 combined force distributions, namely  $\mathbf{p}_U^+$ ,  $\mathbf{p}_U^-$ ,  $\mathbf{p}_V^+$ , and  $\mathbf{p}_V^-$ , are determined:

$$\begin{cases} \mathbf{p}_U^\pm = \mathbf{M}(\Gamma_{1Uie}\Phi_{1ie}A_{1U}^*_{\max} \pm 0.5\Gamma_{2Vie}\Phi_{2ie}A_{2V}^*_{\max}) \\ \mathbf{p}_V^\pm = \mathbf{M}(\pm 0.5\Gamma_{1Uie}\Phi_{1ie}A_{1U}^*_{\max} + \Gamma_{2Vie}\Phi_{2ie}A_{2V}^*_{\max}) \end{cases}. \quad (43)$$

Next, pushover analyses (referred to as pushovers 1U and 2U, respectively) are performed using  $\mathbf{p}_U^+$  and  $\mathbf{p}_U^-$  until the equivalent displacement  ${}_n D_U^*$  calculated from Equation (44) reaches  $D_{1U}^*_{\max}$  as obtained in step 2:

$${}_n D_U^* = \Gamma_{1Uie}\Phi_{1ie}^T \mathbf{M} \mathbf{n} \mathbf{d} / M_{1Uie}^*, \quad (44)$$

$$M_{1Uie}^* = \Gamma_{1Uie}^2 \Phi_{1ie}^T \mathbf{M} \Phi_{1ie}. \quad (45)$$

In Equation (45),  $M_{1Uie}^*$  is the equivalent first modal mass with respect to the  $U$ -axis, and it is determined in terms of  $\Gamma_{1Uie}\Phi_{1ie}$ . Similarly, pushover analyses (referred to as pushovers 1V and 2V, respectively) are performed using  $\mathbf{p}_V^+$  and  $\mathbf{p}_V^-$  until the equivalent displacement  ${}_n D_V^*$  calculated from Equation (46) reaches  $D_{2V}^*_{\max}$  as obtained from step 4:

$${}_n D_V^* = \Gamma_{2Vie}\Phi_{2ie}^T \mathbf{M} \mathbf{n} \mathbf{d} / M_{2Vie}^*. \quad (46)$$

The largest peak response at each frame is determined from the envelope of (i) pushovers 1U and 2U and (ii) pushovers 1V and 2V.

## 3. Numerical Example

### 3.1 Building and ground motion data

#### 3.1.1 Building data

In this study, the 6 four-story asymmetric building models shown in Figure 3 are investigated. In models 1-3, the structural walls are placed at perimeter frames: in model 1, the structural walls are placed at frames Y1, Y4, and X1, whereas in models 2 and 3, they are placed at frames Y1 and X1. In contrast, in models 4-6, most of the structural walls are placed at inner frames. Figure 4 shows the structural elevation of model 1 as an example. The first story is 4.0 m tall, and the upper stories are 3.6 m tall. The compressive strength  $\sigma_B$  of concrete is assumed as 24 N/mm<sup>2</sup>. In addition, SD345 steel (with a yield strength of  $\sigma_y = 345$  N/mm<sup>2</sup>) is used for longitudinal reinforcement and SD295 steel ( $\sigma_y = 295$  N/mm<sup>2</sup>) is used for shear reinforcement. The cross-sections of the beams (from the second floor to the roof) and columns are 350 × 650 mm and 600 × 600 mm, respectively. The structural walls are 220 mm thick. The columns are assumed to be supported at fixed ends by the foundation. The floor mass  $m_j$  and moment of inertia  $I_j$  ( $j = 1-4$ ) are considered as 525 t and 4.37 × 10<sup>4</sup> t·m<sup>2</sup>, respectively. Each frame structure is designed according to the strong column/weak beam concept: the longitudinal reinforcement of the concrete sections is determined so that any potential hinges are located at the ends of beams, the bottom of columns, or the structural walls in the first story. Sufficient shear reinforcement is assumed to be provided to prevent premature shear failure. Table 1 presents the longitudinal reinforcement of each member.

The base shear coefficient when the roof displacement reaches 1/100 of the total height is obtained from the planar pushover analysis. The base shear coefficients for model 1 in each orthogonal direction are 0.532 in the X-direction and 0.455 in the Y-direction; for model 2, they are 0.522 (X) and 0.455 (Y); for model 3, they are 0.421 (X) and 0.455 (Y); for model 4, they are 0.562 (X) and 0.479 (Y); for model 5, they are 0.547 (X) and 0.479 (Y); and for model 6, they are 0.438 (X) and 0.479 (Y). The locations  $e_X$  and  $e_Y$  of the center of stiffness and stiffness eccentricity, respectively, and the radii  $j_X'$  and  $j_Y'$  of torsional stiffness with respect to the center of stiffness are calculated at each story according to the linear static analysis and procedures proposed by Bosco et al.<sup>68</sup> The eccentricity indices  $R_{eX}$  and  $R_{eY}$  ( $= e_Y/j_X'$  and  $e_X/j_Y'$ , respectively) defined by the Building Standard Law of Japan<sup>69</sup> are then calculated for each model. The ranges of  $R_{eX}$  and  $R_{eY}$  in each story are as follows:  $R_{eX} = 0$  and  $R_{eY} = 0.579-0.967$

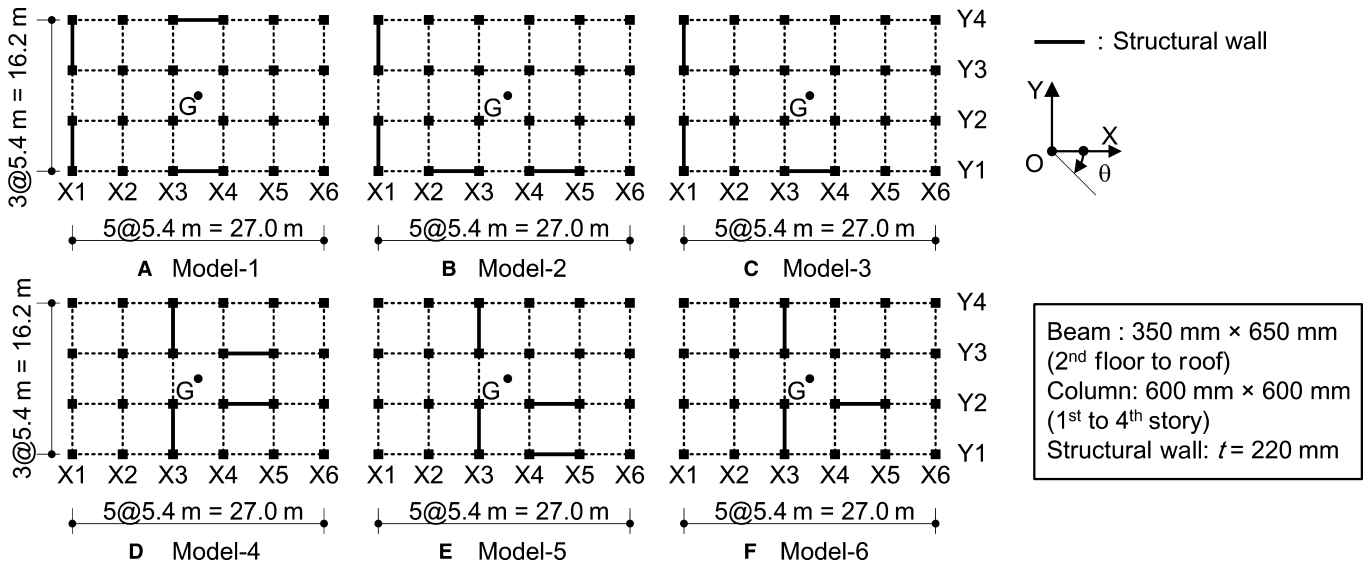


Figure 3. Plan views of 6 model buildings

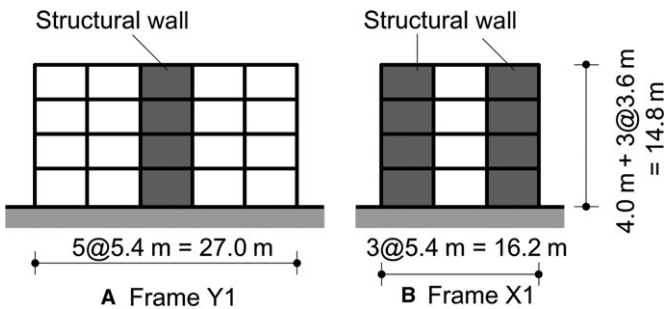


Figure 4. Elevations of building model-1

Table 1. Longitudinal reinforcement of each member

Member	Location	Reinforcement
Boundary beam	2nd floor to roof	6-D25 (top and bottom)
Beam	4th floor and roof	3-D25 (top and bottom)
	2nd to 3rd floor	4-D25 (top and bottom)
Column	2nd to 4th story	20-D29 (top and bottom)
	1st story	20-D29 (top), 8-D29 (bottom)
Structural wall	All stories	D10@200Double

(model 1);  $R_{eX} = 0.345-0.772$  and  $R_{eY} = 0.554-1.252$  (model 2);  $R_{eX} = 0.173-0.507$  and  $R_{eY} = 0.574-1.270$  (model 3);  $R_{eX} = 0$  and  $R_{eY} = 0.151-0.364$  (model 4);  $R_{eX} = 0.285-0.678$  and  $R_{eY} = 0.144-0.339$  (model 5); and  $R_{eX} = 0.065-0.263$  and  $R_{eY} = 0.140-0.400$  (model 6). Note that eccentricity indices  $R_{eX}$ ,  $R_{eY}$  are the largest in the first story and smallest in the fourth story in all building models considered in this paper.

The building structures are modeled as a pseudo 3-dimensional frame model in which the floor diaphragms are assumed to be rigid in their own planes with no out-of-plane stiffness, and the frames oriented in the X- and Y-directions are modeled independently. A one-component model, with one non-linear flexural spring at each end and one non-linear shear spring at the middle of the line element, is used for all beams,

columns, and structural walls. To determine the flexibility of the non-linear flexural springs, an antisymmetric curvature distribution is assumed for the beams and columns, and a uniform curvature distribution is assumed for the structural walls. For the beams (except the boundary beam), the rigid zone length is assumed as half the depth of the intersected column minus one-fourth of the depth of the considered beam itself, while the rigid zone length on the wall-side of the boundary beam is assumed as half the column-center to column-center length of the structural wall. For the columns, the rigid zone length is assumed as half the depth of the intersected beam minus one-fourth of the depth of the considered column itself, while for the structural walls no rigid zone is considered at either end. The effect of the orthogonal beams on the structural wall is not considered.

Figure 5 shows the envelope curve for the force-deformation relationship of each non-linear spring. The envelopes are assumed to be symmetric in both the positive and negative loading directions. The crack moment  $M_c$ , yield moment  $M_y$  of each member, and crack shear strength  $Q_c$  of each structural wall are calculated according to the AIJ Design Guideline.<sup>70</sup> Note that for calculating the crack and yield moments of the columns and structural walls, only the axial force attributed to the vertical load is considered to simplify the analysis. In Figure 5A, the secant stiffness degradation ratio  $\alpha_y$  of the flexural spring at the yield point is assumed to be 0.25 for all beams and columns, based on results obtained using Sugano's equation.<sup>71,72</sup> For the structural walls at the bottom of the first story,  $\alpha_y$  is assumed to be 0.12, and for all other points, it is assumed as 0.19, based on results of a fiber-model sectional analysis. The tangent stiffness degradation ratio  $\alpha_2$  of the flexural spring beyond the yielding point is assumed to be 0.001 for all beams, columns, and structural walls. In Figure 5B, the secant stiffness degradation ratio  $\beta_y$  of the shear spring at the yield point is assumed to be 0.16, based on the results obtained using Sugano's equation.<sup>71,72</sup>

The Muto hysteresis model<sup>73</sup> with 1 modification is used to model the flexural springs, as shown in Figure 6A. Specifically, the unloading stiffness after yielding decreases in proportion to  $\mu^{-0.5}$  ( $\mu$  is the ductility of the flexural spring) to represent the degradation of the unloading stiffness after yielding of the RC



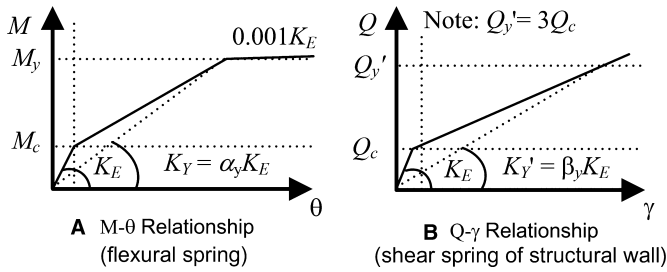


Figure 5. Envelopes of the force-deformation relationship

members, as in the model of Otani.<sup>74</sup> The origin-oriented model (Figure 6B) is used to model the shear spring of a structural wall; the shear springs of beams and columns are assumed to be elastic. The axial stiffness of the columns and walls is assumed to remain elastic, and the effects of biaxial bending and axial-flexural interaction are ignored. The torsional stiffness of the members is also ignored. No second-order effects (eg, the P-Δ effect) are considered. The damping matrix is assumed to be proportional to the instant stiffness matrix, with 3% of the critical damping of the first mode.

Figure 7 shows the natural modes of the building models in the elastic range. Here,  $T_{ie}$  is the  $i$ -th natural period in the elastic range ( $i = 1-3$ );  $\psi_{ie}$  is the angle of incidence of the principal direction of the  $i$ -th modal response in the elastic range; and  $R_{pie}$  is the torsional index of the  $i$ -th mode in the elastic range. As shown in Figure 7 A-C for models 1-3, respectively, the first mode is predominantly translational ( $R_{p1e} = 0.501-0.555 < 1$ ); the second mode is almost purely translational ( $R_{p2e} = 0.000-0.119 \ll 1$ ); and the third mode is predominantly torsional ( $R_{p3e} = 1.584-1.976 > 1$ ). Therefore, these 3 building models are classified as TS. In contrast, as shown in Figure 7D-F for models 4-6, respectively, the first mode is predominantly torsional ( $R_{p1e} = 1.271-2.553 > 1$ ), while the second mode is almost purely translational ( $R_{p2e} = 0.000-0.295 \ll 1$ ), and the third mode is predominantly translational ( $R_{p3e} = 0.385-0.782 < 1$ ). Therefore, these 3 building models are classified here as TF.

In addition, the angles between the principal directions of the first 2 modes are close to  $90^\circ$  in models 1-5:  $\Delta\psi_{12} = 86.1-90.5^\circ$  (models 1-3) and  $\Delta\psi_{12} = 90.0-90.5^\circ$  (models 4 and 5). However,  $\Delta\psi_{12} = 55.1^\circ$  in model 6; therefore, assumption 1 (ie, that the principal directions of the first and second modal responses are almost orthogonal) is not suitable for model 6.

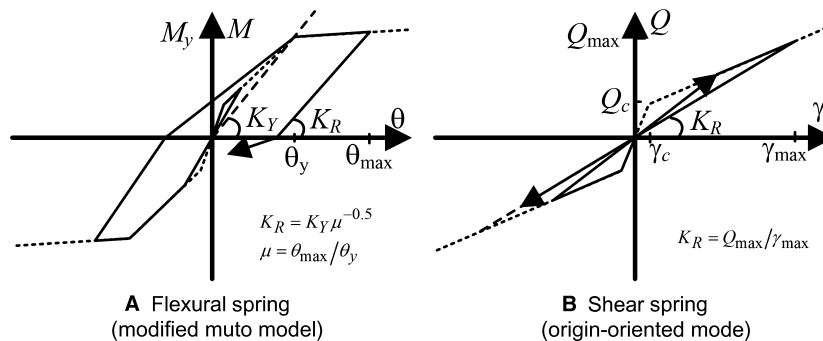


Figure 6. Hysteresis model for the nonlinear spring

### 3.1.2 Ground motion data

In this article, the seismic excitation is bidirectional in the X-Y plane, and 3 sets of artificial ground motions are generated. Note that these 3 sets are the same as those used in a previous work.<sup>53</sup> The response spectra of the major and minor components are assumed to be identical in this work. The target elastic spectrum of the major and minor components with 5% critical damping—namely  $pS_{A\xi}(T, 0.05)$  and  $pS_{A\zeta}(T, 0.05)$ , respectively—as determined from the Building Standard Law of Japan<sup>69</sup> for an extremely rare earthquake event considering type-1 soil (rock) is calculated using Equation (47), where  $T$  represents the natural period of the SDOF model:

$$pS_{A\xi}(T, 0.05) = pS_{A\zeta}(T, 0.05) = \begin{cases} 4.8 + 45T\text{m/s}^2 & : T \leq 0.16\text{s} \\ 12.0 & : 0.16\text{s} < T \leq 0.576\text{s} \\ 12.0(0.576/T) & : T > 0.576\text{s} \end{cases} \quad (47)$$

The phase angle is given by uniform random values and the Jennings-type envelope function  $e(t)$  proposed by the Building Center of Japan<sup>75,76</sup>:

$$e(t) = \begin{cases} (t/5) & : 0\text{s} \leq t \leq 5\text{s} \\ 1 & : 5\text{s} < t \leq 35\text{s} \\ \exp\{-0.027(t - 35)\} & : 35\text{s} < t \leq 120\text{s} \end{cases} \quad (48)$$

Figure 8 shows the elastic response spectra of artificial ground motions with 5% critical damping. Note that the artificial ground motions used in this study are generated independently, that is, there is no correlation between each component. The correlation coefficients of all 3 sets are close to 0, although the envelope functions of the 2 components are the same; therefore, the 2 components can be considered independently of each other.

In this study, the angle of incidence  $\psi$  of the major component with respect to the X-axis is varied at intervals of  $15^\circ$  from  $(\psi_{1ie} - 90)^\circ$  to  $(\psi_{1ie} + 75)^\circ$ , where  $\psi_{1ie}$  is the angle of incidence of the  $U$ -axis corresponding to the predicted peak response  $D_{1U^*max}$  of the first mode. Note that in this study, case  $(\psi_{1ie} + 90)^\circ$  is not included in the time-history analysis cases because that result is identical to that of case  $(\psi_{1ie} - 90)^\circ$ . Therefore,  $3 \times 12 = 36$  cases are considered for the non-linear time-history analyses of each building model.

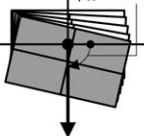
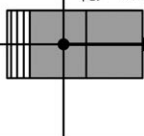
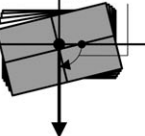
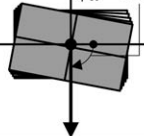
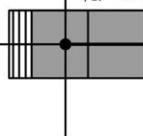
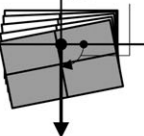
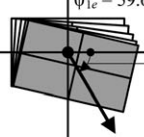
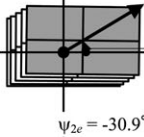
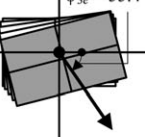
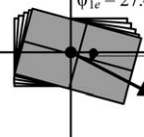
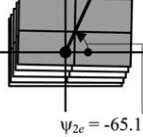
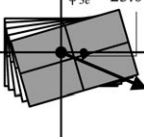
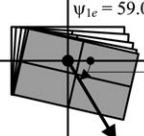
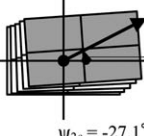
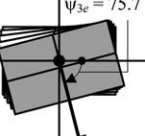
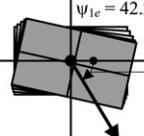
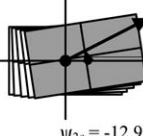
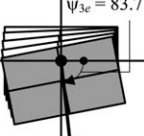
First mode  $\psi_{1e} = 90.0^\circ$	Second mode  $\psi_{2e} = 0.0^\circ$	Third mode  $\psi_{3e} = 90.0^\circ$	First mode  $\psi_{1e} = 90.0^\circ$	Second mode  $\psi_{2e} = 0.0^\circ$	Third mode  $\psi_{3e} = 90.0^\circ$
A Model-1 $T_{1e} = 0.354s, R_{p1e} = 0.501$ $T_{2e} = 0.248s, R_{p2e} = 0.000$ $T_{3e} = 0.149s, R_{p3e} = 1.976$			D Model-4 $T_{1e} = 0.363s, R_{p1e} = 2.553$ $T_{2e} = 0.246s, R_{p2e} = 0.000$ $T_{3e} = 0.243s, R_{p3e} = 0.391$		
First mode  $\psi_{1e} = 59.6^\circ$	Second mode  $\psi_{2e} = -30.9^\circ$	Third mode  $\psi_{3e} = 55.4^\circ$	First mode  $\psi_{1e} = 27.4^\circ$	Second mode  $\psi_{2e} = -65.1^\circ$	Third mode  $\psi_{3e} = 23.0^\circ$
B Model-2 $T_{1e} = 0.435s, R_{p1e} = 0.555$ $T_{2e} = 0.248s, R_{p2e} = 0.023$ $T_{3e} = 0.145s, R_{p3e} = 1.584$			E Model-5 $T_{1e} = 0.380s, R_{p1e} = 1.271$ $T_{2e} = 0.251s, R_{p2e} = 0.037$ $T_{3e} = 0.214s, R_{p3e} = 0.782$		
First mode  $\psi_{1e} = 59.0^\circ$	Second mode  $\psi_{2e} = -27.1^\circ$	Third mode  $\psi_{3e} = 75.7^\circ$	First mode  $\psi_{1e} = 42.2^\circ$	Second mode  $\psi_{2e} = -12.9^\circ$	Third mode  $\psi_{3e} = 83.7^\circ$
C Model-3 $T_{1e} = 0.435s, R_{p1e} = 0.551$ $T_{2e} = 0.293s, R_{p2e} = 0.119$ $T_{3e} = 0.154s, R_{p3e} = 1.655$			F Model-6 $T_{1e} = 0.396s, R_{p1e} = 1.939$ $T_{2e} = 0.294s, R_{p2e} = 0.295$ $T_{3e} = 0.243s, R_{p3e} = 0.385$		

Figure 7. Shapes of the first 3 natural modes of the building models in the elastic range

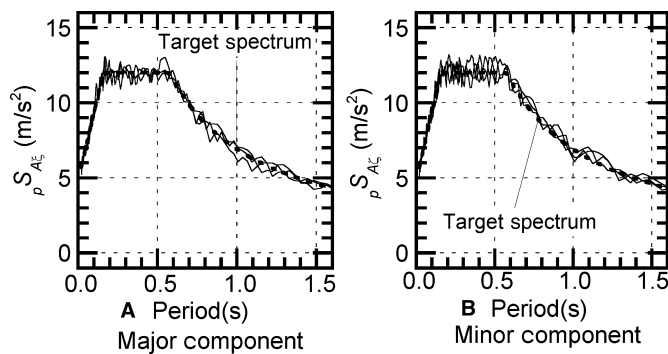


Figure 8. Elastic acceleration response spectra

### 3.2 Prediction of peak responses

Figure 9 shows the predicted peak responses of the equivalent SDOF models representing the first and second modal responses; these responses were obtained by employing the equivalent linearization technique. As shown in this figure, the predicted peak equivalent accelerations  $A_{1U}^*$  of the first mode of models 4 and 6 are higher than those of the other models. This is because, as discussed later, the effective first modal mass of models 4 and 6 is significantly smaller than that of each of the other models.

### 3.3 Comparisons of analysis results

Figure 10 compares the peak displacement at the roof obtained from dynamic analysis results and the predicted peak response for each building model. As shown in Figure 10A-C for models 1-3, respectively, the predicted peak responses agree well with the time-history analysis results except for frame X1. In contrast, as shown in Figure 10D

and F for models 4 and 6, respectively, the predicted peak responses fail to agree with the time-history analysis results; in particular, the predicted peak responses in the Y-direction significantly underestimate the time-history analysis results. Meanwhile, for model 5, as shown in Figure 10E, the predicted peak responses for frames Y1 and Y2 significantly underestimate the time-history analysis results, although the predicted peak responses in the Y-direction agree well with the time-history analysis results.

Figure 11 compares the peak story drift at the flexible side edge frames (frames Y4 and X6) obtained from the time-history analyses and the predicted peak response for each building model. As shown in Figure 11A-C for models 1-3, respectively, the predicted peak responses agree satisfactorily with the time-history analysis results. In contrast, as shown in Figure 11D and F for models 4 and 6, respectively, the predicted peak responses underestimate the average of the time-history analysis results for the flexible edge frame in the X-direction (frame Y4). Meanwhile, for model 5 as shown in Figure 11E, the predicted peak responses agree well with the time-history analysis results for both flexible side edge frames.

## 4. Applicability of the Equivalent SDOF Model Based on the Torsional Index

The numerical results shown above indicate that the predicted peak responses agree well with the time-history analysis results for models 1-3, which are classified as TS in the elastic range. Meanwhile, for models 4-6, which are classified as TF in the elastic range, the accuracy of the predicted results is not as good. In the following paragraphs, the suitability of the presented MABPA for the 6 building models is examined based on the torsional index  $R_{pi}$  of each mode.

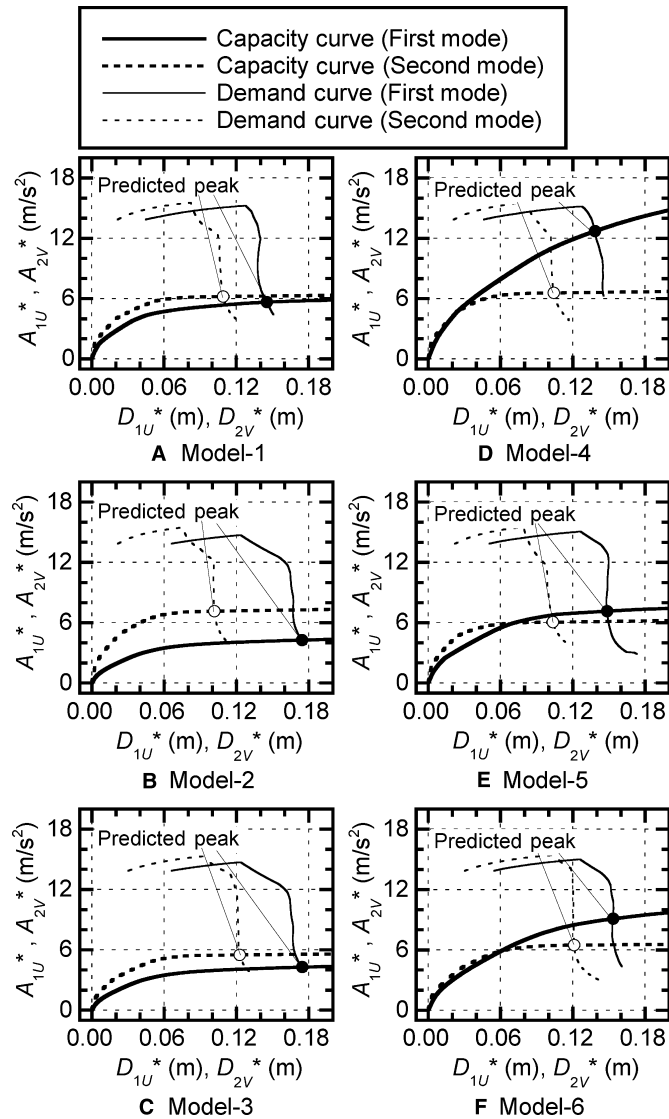


Figure 9. Predicted peak responses of equivalent 5DOF models

From the DB-MAP analysis in MABPA step 1, the second and third mode vectors at step  $n$ — ${}_n\phi_2$  and  ${}_n\phi_3$ , respectively—are calculated in terms of the displacement vector  ${}_n\mathbf{d}$  at step  $n$  and the second and third mode vectors— $\phi_{2e}$  and  $\phi_{3e}$ , respectively—in the elastic range:

$${}_n\phi_2 = \phi_{2e} - \frac{\phi_{2e}^T \mathbf{M}_n \phi_1}{{}_n\phi_1^T \mathbf{M}_n \phi_1} {}_n\phi_1 = \phi_{2e} - \frac{\phi_{2e}^T \mathbf{M}_n \mathbf{d}}{{}_n\mathbf{d}^T \mathbf{M}_n \mathbf{d}} {}_n\mathbf{d}, \quad (49)$$

$${}_n\phi_3 = \phi_{3e} - \frac{\phi_{3e}^T \mathbf{M}_n \mathbf{d}}{{}_n\mathbf{d}^T \mathbf{M}_n \mathbf{d}} {}_n\mathbf{d} - \frac{\phi_{3e}^T \mathbf{M}_n \phi_2}{{}_n\phi_2^T \mathbf{M}_n \phi_2} {}_n\phi_2. \quad (50)$$

Next, the torsional index  ${}_nR_{pi}$  of the  $i$ -th mode at loading step  $n$  and the cosine of the angle  $\Delta_n\psi_{12}$  between the principal direction of the first and second modes at step  $n$  are calculated:

$${}_nR_{pi} = \sqrt{\sum_j I_{jn} \phi_{\Theta ji}^2} / \left( \sum_j m_{jn} \phi_{Xji}^2 + \sum_j m_{jn} \phi_{Yji}^2 \right), \quad (51)$$

$$\cos \Delta_n\psi_{12} = \frac{\left( \sum_j m_j \phi_{Xj1} \right) \left( \sum_j m_j \phi_{Xj2} \right) + \left( \sum_j m_j \phi_{Yj1} \right) \left( \sum_j m_j \phi_{Yj2} \right)}{\sqrt{\left( \sum_j m_j \phi_{Xj1} \right)^2 + \left( \sum_j m_j \phi_{Yj1} \right)^2} \sqrt{\left( \sum_j m_j \phi_{Xj2} \right)^2 + \left( \sum_j m_j \phi_{Yj2} \right)^2}}. \quad (52)$$

Figure 12 shows the change in  ${}_nR_{pi}$  at each loading step of each building model. The dots “●” in this figure correspond to the predicted peak responses  $D_{1U}^*$  of the first mode, as estimated by MABPA.

As shown in Figure 12A for model 1,  ${}_nR_{p1}$  is 0.501-0.621,  ${}_nR_{p2}$  is constantly 0, and  ${}_nR_{p3}$  is 1.60-1.97. As shown in Figure 12B for model 2,  ${}_nR_{p1}$  is 0.555-0.591,  ${}_nR_{p2}$  is 0.023-0.033, and  ${}_nR_{p3}$  is 1.50-1.58. A similar trend can be found in Figure 12C for model 3. In contrast, as shown in Figure 12D-F for models 4-6, respectively,  ${}_nR_{p1}$  is greater than 1.0 from the elastic range to the predicted peak: for models 4 and 6 in

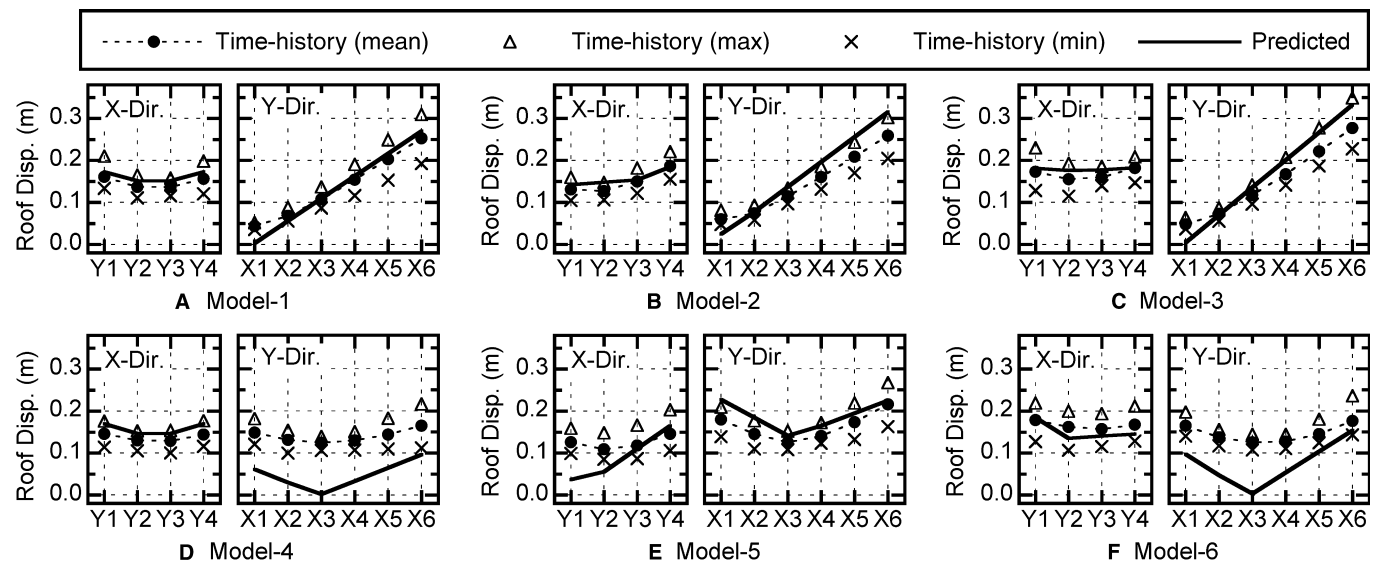


Figure 10. Comparisons of the peak roof displacement at each frame

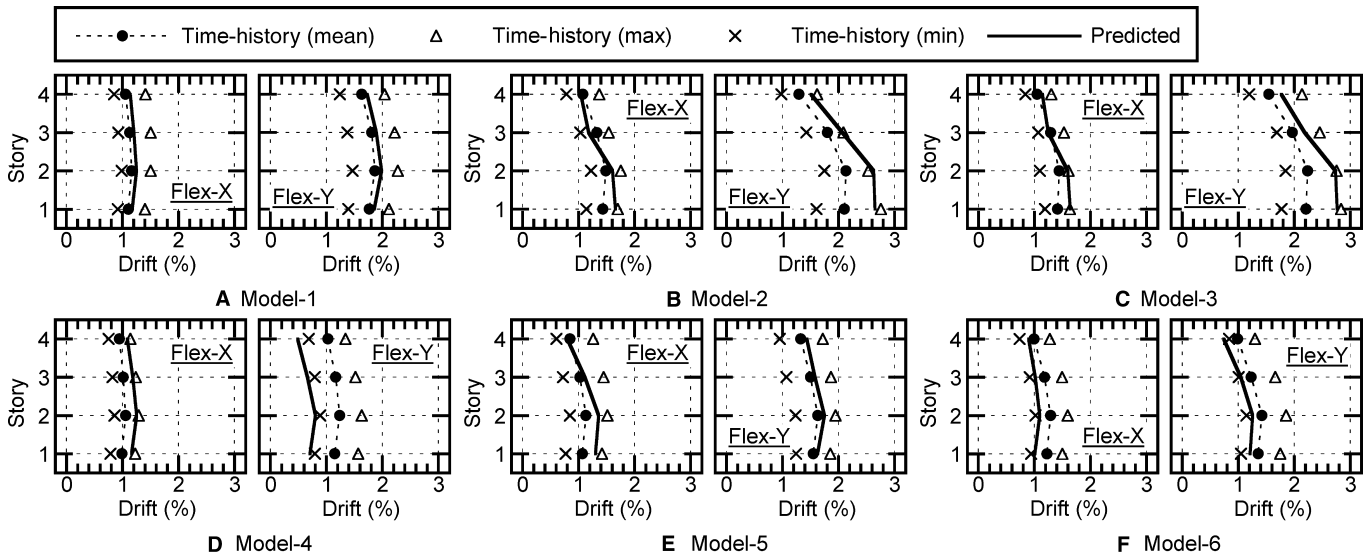


Figure 11. Comparisons of peak story drift at flexible edge frames

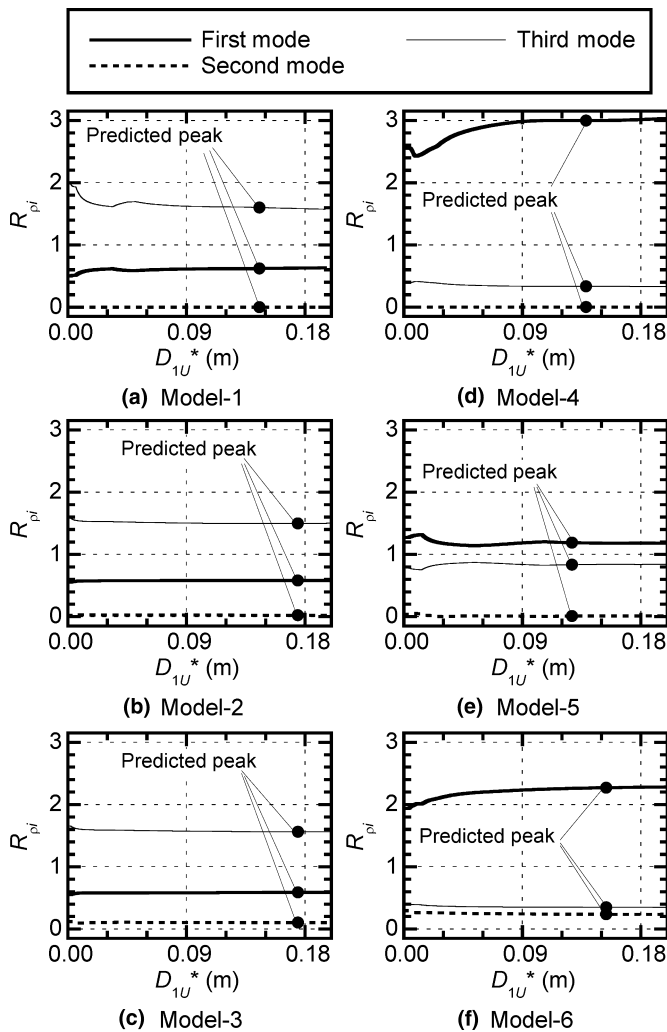


Figure 12. Variations in  $R_{pi}$  based on the pushover analysis

particular,  $nR_{p1}$  corresponds to the predicted peaks at 3.00 and 2.27, respectively. Therefore, models 1-3 are classified as TS from the elastic range to the predicted peak, whereas the others are classified as TF.

Figure 13 shows  $|\cos\Delta_n\psi_{12}|$  and the product  $nR_{p1n}R_{p2}$  evaluated from the pushover analysis results for each building model. As shown in Figure 13A-C for models 1-3, respectively, the values of  $|\cos\Delta_n\psi_{12}|$  are very small ( $< 0.06$ ) from the elastic range to the predicted peak. This implies that the angle  $\Delta_n\psi_{12}$  varies within the range  $86.6\text{-}93.5^\circ$ . Therefore, models 1-3, which are classified as TS, satisfy the condition that the principal directions of the first and second modes are close to orthogonal throughout the response. Similarly, as shown in Figure 13D and E for models 4 and 5, respectively, the values of  $|\cos\Delta_n\psi_{12}|$  are very small ( $< 0.02$ ) from the elastic range to the predicted peak. Therefore, for models 4 and 5, the principal directions of the first and second modes are close to orthogonal. However, as shown in Figure 13F for model 6,  $|\cos\Delta_n\psi_{12}|$  within 0.5-0.6, which implies that  $\Delta_n\psi_{12}$  varies within the range  $53.1\text{-}60.0^\circ$ . Therefore, model 6 is the only model that does not satisfy the condition that the principal directions of the first and second modes should be close to orthogonal throughout the response.

Note that as shown in Figure 13A-F, the behavior of the product  $nR_{p1n}R_{p2}$  agrees well with that of  $|\cos\Delta_n\psi_{12}|$ . This implies that Equation (31) is valid for the building models considered in this article, and therefore that Equation (31) is useful for evaluating the orthogonality of the principal directions of the first and second modes.

Figure 14 shows the effective modal mass ratios  $m_{1U}^{*ie}$  and  $m_{2V}^{*ie}$  corresponding to the predicted peak  $D_{1U}^{*max}$ . For models 1-3,  $m_{1U}^{*ie}$  is 0.605-0.666, and  $m_{2V}^{*ie}$  is 0.784-0.787. Therefore, these 3 TS building models satisfy the condition that the models oscillate predominantly in the first mode under U-directional excitation and predominantly in the second mode under V-directional excitation. In contrast,  $m_{1U}^{*ie}$  is 0.084-0.358 for models 4-6. Therefore, for these TF building models, the contribution of the responses of higher modes may be significant under U-directional excitation. In addition,  $m_{2V}^{*ie}$  is 0.545 for model 6, which is the smallest value for all the

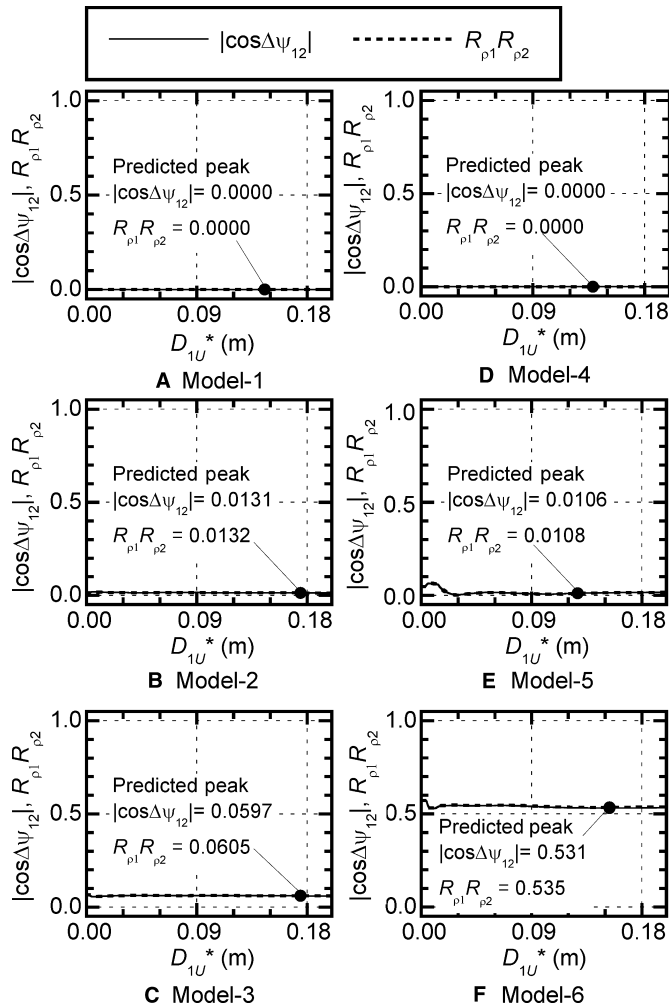


Figure 13. Variations in  $|\cos\Delta\psi_{12}|$  based on the pushover analysis

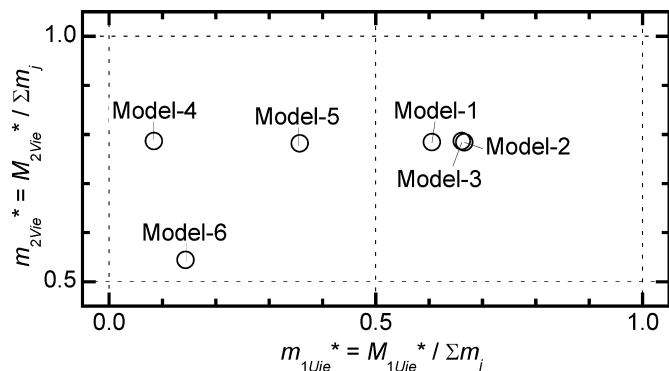


Figure 14. Equivalent modal mass ratios at the peak response

models. This is attributed to the fact that the principal directions of the first and second modes are not orthogonal.

In conclusion, the 3 building models whose peak responses are predicted satisfactorily by MABPA<sup>53</sup> are classified as TS buildings from the elastic range to the peak response. In contrast, the models whose peak responses are underestimated by MABPA are classified as TF buildings. The reasons why the MABPA prediction fails for the TF buildings are that (i) the principal directions of the first and second

modes may not be orthogonal, and (ii) the contribution of higher modes is significant.

### 5. Discussions and Conclusions

In this article, the theoretical background of MABPA, which was proposed earlier by the author,<sup>53</sup> was summarized, and the relationship between its applicability and the torsional indices,  $R_{p1}$ ,  $R_{p2}$ , and  $R_{p3}$ , of the first 3 modes was discussed. Non-linear time-history analyses were performed numerically for 6 four-story RC asymmetric frame buildings with regular elevations under various directions of seismic input, and the results were compared with theoretical predictions. The primary findings of the present study are summarized as follows.

1. The fundamental assumptions of MABPA—(i) the principal directions of the first and second modal responses are almost orthogonal and (ii) the building oscillates predominantly in each orthogonal direction—are strongly related to the torsional indices  $R_{p1}$  and  $R_{p2}$ . If both assumptions are applicable to an asymmetric building, it must be a TS building that satisfies the conditions  $R_{p1}, R_{p2} < 1$  and  $R_{p3} > 1$ .
2. For the 6 asymmetric building models investigated herein, the peak response was predicted satisfactorily by MABPA for those building models classified as TS from the elastic range to the predicted peak response. However, for those building models classified as TF, the results predicted by MABPA were significantly underestimated compared to the time-history analysis results. This was because (i) the principal directions of the first and second modes may not have been orthogonal, and (ii) the contribution of higher modes was significant.

Based on the primary findings above, the application of MABPA should be limited to building model classified as TS: the torsional indices,  $R_{p1}$ ,  $R_{p2}$ , and  $R_{p3}$ , are key parameters to evaluate the applicability of MABPA. Note that the conclusions drawn here are limited to an asymmetric building model with regular elevation that is designed according to the weak beam/strong column concept. However, as shown in a previous work,<sup>55</sup> the peak response of an asymmetric building with bidirectional setbacks that satisfies the conditions  $R_{p1}, R_{p2} < 1$  and  $R_{p3} > 1$  is successfully predicted by MABPA. Therefore, the conclusions drawn here can be extended to more general irregular buildings. Further work is needed to determine the applicability criteria of MABPA. Future work can aim to improve the prediction accuracy at the stiff-side frames by considering the third and higher modes.

### Disclosure

The authors have no conflict of interest to declare.

### References

- 1 AIJ. Report on the damage investigation of the 1968 Tokachi-oki Earthquake, 1968 (in Japanese).
- 2 AIJ. Report on the damage investigation of the 1978 Miyagiken-oki Earthquake, 1980 (in Japanese).
- 3 Editorial Committee for the Report on the Hanshin-Awaji Earthquake Disaster. Report on the Hanshin-Awaji Earthquake Disaster: Report on the Hanshin-Awaji earthquake disaster, Building series volume 1, Structural damage to reinforced concrete building, 1997 (in Japanese).
- 4 Saiidi M, Sozen MA. Simple nonlinear seismic analysis of R/C structures. *J Struct Div ASCE*. 1981;107:937-952.

- 5 Fajfar P, Fischinger M. N2-a method for non-linear seismic analysis of regular buildings. In: Proceedings of ninth world conference on earthquake engineering, Vol. V:111-116, Tokyo-Kyoto, Japan, 1988.
- 6 Fajfar P. A nonlinear analysis method for performance-based seismic design. *Earthq Spectra*. 2000;**16**:573-592.
- 7 ATC-40. *Seismic Evaluation and Retrofit of Concrete Buildings*, Vol. 1. Redwood City, CA: Applied Technology Council; 1996.
- 8 FEMA. *NEHRP Guidelines for the Seismic Rehabilitation of Buildings*, FEMA Publication 273. Washington, DC: Federal Emergency Management Agency; 1997.
- 9 CEN. Eurocode 8 - design of structures for earthquake resistance. Part 1: general rules, seismic actions and rules for buildings. European standard EN 1998-1. Brussels: European Committee for Standardization; 2004.
- 10 ASCE. *Seismic Rehabilitation of Existing Buildings*. Reston, VA: American Society of Civil Engineering; 2007.
- 11 González P. Considering earthquake direction on seismic analysis. In: Proceedings of the Tenth World Conference on Earthquake Engineering, 7: 3809-3913, Madrid, Spain, 1992.
- 12 Chow YD, Sera K, Nishilawa T. Torsional response analysis of the damaged reinforced concrete building (Analysis of the Hachinohe Library Building). Summaries of Technical Papers of Annual Meeting, Architectural Institute of Japan, Volume B, 915-916, 1989 (in Japanese).
- 13 Chow YD, Sera K, Nishilawa T. Inelastic response analyses of structures with torsion. In: Proceedings of the Eighth Japan Earthquake Symposium, 1665-1669, 1990 (in Japanese).
- 14 Sudo S, Sera K, Nishilawa T. On the torsional response analyses of buildings subjected to bi-directional ground motions. In: Proceedings of the Ninth Japan Earthquake Symposium, 1597-1602, 1994 (in Japanese).
- 15 Sudo S, Sera K, Nishikawa T. Torsional response analysis of buildings subjected to bi-directional ground motions. In: Proceedings of the Eleventh World Conference on Earthquake Engineering, Paper No. 865, Acapulco, Mexico, 1996.
- 16 Sakata M, Yamamura K, Nishikawa T. Analyses on torsional response of multi-story space frames to bi-directional earthquake ground motion. Summaries of Technical Papers of Annual Meeting, Architectural Institute of Japan, Volume B, 439-440, 2000.9 (in Japanese).
- 17 Yamanaka N, Yoshimura M. Torsional response of one-story frame structures with wall subjected to earthquake motions with arbitrary direction. In: Proceedings of the Tenth Japan Earthquake Symposium, 2601-2606, 1998 (in Japanese).
- 18 López A, Torres R. The critical angle of seismic incidence and the maximum structural response. *Earthq Eng Struct Dyn*. 1997;**26**:881-894.
- 19 Kostinakis KG, Athanatopoulou AM, Avramidis IE. Evaluation of inelastic response of 3D single-story R/C frames under bi-directional excitation using different orientation schemes. *Bull Earthq Eng*. 2013;**11**:637-661.
- 20 Kappos AJ, Perdikoulis KA. Effect of angle of incidence of seismic waves on the inelastic dynamic response of irregular R/C structures. In: Sixth European workshop on the seismic behaviour of irregular and complex structures, Paper No. 32, Haifa, Israel, 2011.
- 21 Magliulo G, Maddaloni G, Petrone C. Influence of earthquake direction on the seismic response of irregular plan RC frame buildings. *Earthq Eng Vib*. 2014;**13**:243-256.
- 22 Fontara IM, Kostinakis KG, Manoukas GE, Athanatopoulou AM. Parameters affecting the seismic response of buildings under bi-directional excitation. *Struct Eng Mech*. 2015;**53**:957-979.
- 23 Reyes JC, Kalkan E. Significance of rotating ground motions on behavior of symmetric- and asymmetric-plan structures: part I. Single-story structures. *Earthq Spectra*. 2015;**31**:1591-1612.
- 24 Kalkan E, Reyes JC. Significance of rotating ground motions on behavior of symmetric- and asymmetric-plan structures: part II. Multi-story structures. *Earthq Spectra*. 2015;**31**:1613-1628.
- 25 Fujii K, Ikeda T. Shaking table test of irregular buildings under horizontal excitation acting in an arbitrary direction. In: Proceedings of 15th world conference on earthquake engineering, Paper No. 0439, Lisbon, Portugal, 2012.
- 26 Moghadam AS, Tso WK. Damage assessment of eccentric multistorey buildings using 3-D pushover analysis. In: Proceedings of 11th world conference on earthquake engineering, Paper No. 997, Acapulco, Mexico, 1996.
- 27 Moghadam AS, Tso WK. Pushover analysis for asymmetric and set-back multi-story buildings. Proceedings of 12th world conference on earthquake engineering, Auckland, New Zealand, February, 2000.
- 28 Perus I, Fajfar P. On the inelastic torsional response of single-storey structures under bi-axial excitation. *Earthq Eng Struct Dyn*. 2005;**34**:931-941.
- 29 Fajfar P, Marusić D, Perus I. Torsional effects in the pushover-based seismic analysis of buildings. *J Earthq Eng*. 2005;**9**:831-854.
- 30 D'Ambrisi A, De Stefano M, Tanganelli M. Use of pushover analysis for predicting seismic response of irregular buildings: a case study. *J Earthq Eng*. 2009;**13**:1089-1100.
- 31 Kreslin M, Fajfar P. Seismic evaluation of an existing complex RC building. *Bull Earthq Eng*. 2010;**8**:363-385.
- 32 Kreslin M, Fajfar P. The extended N2 method considering higher mode effects in both plan and elevation. *Bull Earthq Eng*. 2012;**10**:695-715.
- 33 Bhatt C, Bento R. Assessing the seismic response of existing RC buildings using the extended N2 method. *Bull Earthq Eng*. 2011;**9**:1183-1201.
- 34 Bhatt C, Bento R. Comparison of nonlinear static methods for the seismic assessment of plan irregular frame buildings with non seismic details. *J Earthq Eng*. 2012;**16**:15-39.
- 35 Bhatt C, Bento R. The extended adaptive capacity spectrum method for the seismic assessment of plan-asymmetric buildings. *Earthq Spectra*. 2014;**30**:683-703.
- 36 Cimellaro GP, Giovine T, Lopez-Garcia D. Bidirectional pushover analysis of irregular structures. *J Struct Eng*. 2014;**140**:04014059. [https://doi.org/10.1061/\(ASCE\)ST.1943-541X.0001032](https://doi.org/10.1061/(ASCE)ST.1943-541X.0001032).
- 37 Chopra AK, Goel RK. A modal pushover analysis procedure to estimate seismic demands for unsymmetric-plan buildings. *Earthq Eng Struct Dyn*. 2004;**33**:903-927.
- 38 Reyes JC, Chopra AK. Three-dimensional modal pushover analysis of buildings subjected to two components of ground motion, including its evaluation for tall buildings. *Earthq Eng Struct Dyn*. 2011;**40**:789-806. <https://doi.org/10.1002/eqe.1060>.
- 39 Reyes JC, Chopra AK. Evaluation of three-dimensional modal pushover analysis for unsymmetric-plan buildings subjected to two components of ground motion. *Earthq Eng Struct Dyn*. 2011;**40**:1475-1494. <https://doi.org/10.1002/eqe.1100>.
- 40 Manoukas G, Athanatopoulou A, Avramidis I. Multimode pushover analysis for asymmetric buildings under biaxial seismic excitation based on a new concept of the equivalent single degree of freedom system. *Soil Dyn Earthq Eng*. 2012;**38**:88-96. <https://doi.org/10.1016/j.soildyn.2012.01.018>.
- 41 Manoukas G, Avramidis I. Evaluation of a multimode pushover procedure for asymmetric in plan buildings under biaxial seismic excitation. *Bull Earthq Eng*. 2014;**12**:2607-2632.
- 42 Belejo A, Bento R. Improved modal pushover analysis in seismic assessment of asymmetric plan buildings under the influence of one and two horizontal components of ground motions. *Soil Dyn Earthq Eng*. 2016;**87**:1-15. <https://doi.org/10.1016/j.soildyn.2016.04.011>.
- 43 Soleimani S, Aziminejad A, Moghadam AS. Extending the concept of energy-based pushover analysis to assess seismic demands of asymmetric-plan buildings. *Soil Dyn Earthq Eng*. 2017;**93**:29-41. <https://doi.org/10.1016/j.soildyn.2016.11.014>.
- 44 Bosco M, Gherzi A, Marino EM. Corrective eccentricities for assessment by nonlinear static method of 3D structures subjected to bidirectional ground motion. *Earthq Eng Struct Dyn*. 2012;**41**:1751-1773.
- 45 Bosco M, Ferrara GAF, Gherzi A, Marino EM, Rossi PP. Predicting displacement demand of multi-storey asymmetric buildings by nonlinear static analysis and corrective eccentricities. *Eng Struct* 2015;**99**:373-387. <https://doi.org/10.1016/j.engstruct.2015.05.006>.
- 46 Fujii K, Nakano Y, Sanada Y. Equivalent SDOF model for asymmetric buildings subjected to bi-directional ground motion. *Concr Res Technol*. 2005;**16**:37-47 (in Japanese).
- 47 Fujii K, Nakano Y, Sanada Y, Sakata H, Wada A. Prediction of seismic response of single-story unsymmetric buildings using equivalent SDOF model and its applicability. *J Struct Constr Eng*. 2005;**596**:101-108 (in Japanese).
- 48 Fujii K, Nakano Y. Prediction of seismic response of multi-story unsymmetric frame buildings. *J Struct Constr Eng*. 2006;**607**:149-156 (in Japanese).
- 49 Fujii K. Prediction of largest peak seismic response at flexible-side frame of asymmetric buildings under horizontal ground motion act in arbitrary direction. *J Struct Constr Eng*. 2010;**77**:1247-1256 (in Japanese).
- 50 Fujii K. Nonlinear static procedure for multi-story asymmetric frame buildings considering bi-directional excitation. *J Earthq Eng*. 2011;**15**:245-273.
- 51 Fujii K. Seismic performance evaluation of existing R/C asymmetric buildings considering the direction of seismic input. *J Struct Constr Eng*. 2012;**77**:565-574 (in Japanese).
- 52 Fujii K. Torsional index of single-story asymmetric building model for application of seismic response evaluation using equivalent SDOF model. *J Struct Constr Eng*. 2013;**78**:299-308 (in Japanese).
- 53 Fujii K. Prediction of the largest peak nonlinear seismic response of asymmetric buildings under bi-directional excitation using pushover analyses. *Bull Earthq Eng*. 2014;**12**:909-938.
- 54 Fujii K. Application of the pushover-based procedure to predict the largest peak response of asymmetric buildings with buckling-restrained braces. 5th International conference on computational methods in structural dynamics and earthquake engineering (COMPDYN 2015), Crete Island, Greece, May, 2015. <https://doi.org/10.7712/120115.3654.836>.
- 55 Fujii K. Assessment of pushover-based method to a building with bidirectional setback. *Earthq Struct*. 2016;**11**:421-443. <https://doi.org/10.12989/eas.2016.11.3.421>.
- 56 Lavan O, De Stefano M, eds. *Seismic Behaviour and Design of Irregular and Complex Civil Structures*. Dordrecht: Springer; 2013.

- 57 Zembaty Z, De Stefano M, eds. *Seismic Behaviour and Design of Irregular and Complex Civil Structures II*. Dordrecht: Springer; 2016.
- 58 De Stefano M, Pintucchi B. A review on seismic behaviour of irregular building structure since 2002. *Bull Earthq Eng*. 2008;**6**:285-308.
- 59 Anagnostopoulos SA, Kyrkos MT, Stathopoulos KG. Earthquake induced torsion in buildings: critical review and state of the art. *Earthq Struct*. 2015;**8**:305-377. <https://doi.org/10.12989/eas.2015.8.2.305>.
- 60 De Stefano M, Pintucchi B. Predicting torsion-induced lateral displacements for pushover analysis: influence of torsion system characteristics. *Earthq Eng Struct Dyn*. 2010;**39**:1369-1394.
- 61 Isakovic T, Fischinger M. Applicability of pushover methods to the seismic analysis of an RC bridge, experimentally tested on three shake tables. *J Earthq Eng*. 2011;**15**:303-320.
- 62 Chopra AK, Goel RK. A modal pushover analysis procedure for estimating seismic demands for buildings. *Earthq Eng Struct Dyn*. 2002;**31**:561-582.
- 63 Fujii K. Torsional index of an asymmetric building based on mode shape. In: Zembaty Z, De Stefano M, eds. *Seismic Behaviour and Design of Irregular and Complex Civil Structures II*. Dordrecht: Springer; 2016:99-109.
- 64 Hejal R, Chopra AK. Earthquake response of torsionally-coupled buildings. Earthquake Engineering Research Center, Report no. UCB/EERC-87/20, College of Engineering, University of California at Berkeley, 1987.
- 65 Otani S. New seismic design provision in Japan. In: Proceeding of the second U.S.-Japan workshop on performance-based earthquake engineering methodology for reinforced concrete structures, PEER Report 2000/10: 3-14, 2000.
- 66 Building Guidance Division, Housing Bureau, Ministry of Land, Infrastructure and Transport. 2001 guidelines and examples for calculation of response and limit capacity, Kougaku-tosho, 2001 (in Japanese).
- 67 Yoshilawa K, Okano H, Koshika N. Evaluation of earthquake response of single-story unsymmetric buildings by equivalent linearization method considering higher mode. *J Struct Constr Eng*. 2007;**621**:57-65 (in Japanese).
- 68 Bosco M, Marino EM, Ghersi A. An analytical method for evaluation of the in-plan irregularity of non-regularly asymmetric buildings. *Bull Earthq Eng*. 2013;**11**:1423-1445. <https://doi.org/10.1007/s10518-013-9438-3>.
- 69 BCJ. *The Building Standard Law of Japan on CD-ROM*. Tokyo: The Building Center of Japan; 2016.
- 70 AIJ. *Design Guidelines for Earthquake Resistant Reinforced Concrete Buildings Based on Inelastic Displacement Concept*. Tokyo: Architectural Institute of Japan; 1999 (in Japanese).
- 71 Sugano S. Experimental study on restoring force characteristics of reinforced concrete members. *Concr J*. 1973;**11**:1-9 (in Japanese).
- 72 Sugano S, Koreishi I. An empirical evaluation of inelastic behaviour of structural elements in reinforced concrete frames subjected to lateral forces. In: Proceedings of the fifth world conference on earthquake engineering. 1: 841-844, Rome, Italy, 1974.
- 73 Muto K, Hisada T, Tsugawa T, Bessho S. Earthquake resistant design of a 20 story reinforced concrete buildings. In: Proceedings of the fifth world conference on earthquake engineering, 2: 1960-1969, Rome, Italy, 1974.
- 74 Otani S. Hysteresis models of reinforced concrete for earthquake response analysis. *J Faculty Eng*. 1981;**36**:125-156.
- 75 BRI, BCJ. Guideline for the generation of earthquake motions for seismic design of buildings (draft), 1993 (in Japanese).
- 76 Otani S. Japanese Seismic Design of High-Rise Reinforced Concrete Buildings - An Example of Performance-Based Design Code and State of Practices. In: Proceedings of the 13th world conference on earthquake engineering, Paper No. 5010, Vancouver, Canada, 2004.

**How to cite this article:** Fujii K. Prediction of the peak seismic response of asymmetric buildings under bidirectional horizontal ground motion using equivalent SDOF model. *Jpn Archit Rev*. 2018;**1**:29-43. <https://doi.org/10.1002/2475-8876.1007>